Copyright Warning & Restrictions

The copyright law of the United States (Title 17, United States Code) governs the making of photocopies or other reproductions of copyrighted material.

Under certain conditions specified in the law, libraries and archives are authorized to furnish a photocopy or other reproduction. One of these specified conditions is that the photocopy or reproduction is not to be "used for any purpose other than private study, scholarship, or research." If a, user makes a request for, or later uses, a photocopy or reproduction for purposes in excess of "fair use" that user may be liable for copyright infringement,

This institution reserves the right to refuse to accept a copying order if, in its judgment, fulfillment of the order would involve violation of copyright law.

Please Note: The author retains the copyright while the New Jersey Institute of Technology reserves the right to distribute this thesis or dissertation

Printing note: If you do not wish to print this page, then select "Pages from: first page # to: last page #" on the print dialog screen

ABSTRACT

MICROWAVE HEATING OF FLUID/SOLID LAYERS: A STUDY OF HYDRODYNAMIC STABILITY AND MELTING FRONT PROPAGATION

by
John Gilchrist

In this work we study the effects of externally induced heating on the dynamics of fluid layers, and materials composed of two phases separated by a thermally driven moving front. One novel aspect of our study, is in the nature of the external source which is provided by the action of microwaves acting on dielectric materials. The main challenge is to model and solve systems of differential equations which couple fluid dynamical motions (the Navier-Stokes equations for non-isothermal flows) and electromagnetic wave propagation (governed by Maxwell's equations).

When an electromagnetic wave impinges on a material, energy is generated within the material due to dipolar and ohmic heating. The electrical and thermal properties of the material dictate the dynamics of the heating process, as well as steady-state temperature profiles. Such forms of heating have received little attention in studies of hydrodynamic instabilities of non-isothermal flows, such as the classical Bénard problem, for instance. The novel feature, which allows possibilities for fluid management and control, is the non-local coupling between the electromagnetic field and the temperature distribution within the fluid. In the first part of the thesis, we consider hydrodynamic instabilities of such systems with particular emphasis on conditions for onset of convection. This is achieved by solving the linear stability equations in order to identify parameter values which produce instability. The analysis and subsequent numerical solutions are carried out both for materials with constant dielectric attributes (in such cases the electric field equations decouple and they can be solved in closed form), and materials with temperature dependent

MICROWAVE HEATING OF FLUID/SOLID LAYERS: A STUDY OF HYDRODYNAMIC STABILITY AND MELTING FRONT PROPAGATION

by
John Gilchrist

A Dissertation
Submitted to the Faculty of
New Jersey Institute of Technology
in Partial Fulfillment of the Requirements for the Degree of
Doctor of Philosophy

Department of Mathematics

August 1998

APPROVAL PAGE

MICROWAVE HEATING OF FLUID/SOLID LAYERS: A STUDY OF HYDRODYNAMIC STABILITY AND MELTING FRONT PROPAGATION

John Gilchrist

Gregory A. Kriegsmann, Ph.D., Dissertation Advisor — Date
Distinguished Professor, Department of Mathematics,
New Jersey Institute of Technology, Newark NJ

Demetrius Papageorgiou, Ph.D., Dissertation Advisor — Date
Associate Professor, Department of Mathematics,
New Jersey Institute of Technology, Newark NJ

Jonathan H. C. Luke, Ph.D., Committee Member — Date
Associate Professor, Department of Mathematics,
New Jersey Institute of Technology, Newark NJ

Yuriko Renardy, Ph.D., Committee Member — Date
Professor, Department of Mathematics,
Virginia Polytechnic Institute and State University, Blacksburg VA

Burt S. Tilley, Ph.D., Committee Member — Date
Assistant Professor, Department of Mathematics,
New Jersey Institute of Technology, Newark NJ

BIOGRAPHICAL SKETCH

Author: John Gilchrist

Degree: Doctor of Philosophy

Date: August 1998

Undergraduate and Graduate Education:

- Doctor of Philosophy in Applied Mathematics,
  New Jersey Institute of Technology, Newark, NJ, 1998
- Master of Science in Applied Mathematics,
  New Jersey Institute of Technology, Newark, NJ, 1991
- Batchelor of Science in Computer Science,
  Rutgers University (Cook College), New Brunswick, NJ, 1986

Major: Applied Mathematics

Publications:

John J. Gilchrist, Gregory A. Kriegsmann, Demetrius Papageorgiou, "Stability of A Microwave Heated Fluid Layer", *IMA Journal of Applied Mathematics*, January 1998.

John J. Gilchrist, C. Musante, S. Nanda, J. Rodricks, D. Trubatch, "Modeling of Thin Filaments of Polymeric Liquid Crystals", *Claremont Colleges Mathematics Modeling Workshop Proceedings*, Claremont, CA, June, 1994.

To my parents

ACKNOWLEDGMENT

I, in all probability, never would have pursued a doctoral degree without the inspiration and encouragement of two very special people, Professor Demetrius Papageorgiou and Professor Gregory A. Kriegsmann, who saw in me talents and abilities that I didn't see in myself. I would like to thank Professor Jonathan Luke, Professor Yuriko Renardy and Professor Burt S. Tilley who where always there to offer me guidance in my research. Their words were always words of encouragement and these words provided me with the strength to endure the tough times. I would like to thank my family who offered their constant support and encouragement. Thanks to my friends who helped me to maintain a proper balance between work and play. They helped me to maintain my sanity during these years of intense work.

TABLE OF CONTENTS

LIST OF FIGURES

CHAPTER 1

INTRODUCTION

1.1 Hydrodynamic Stability

When most fluids are heated, their densities decrease. If the temperature profile is such that a more dense fluid lies over a less dense fluid, then we have a potentially unstable situation in the presence of a gravitational field. In the present study we wish to determine the effects of microwaves on the temperature profile of a given dielectric fluid and, consequently, their effect on the velocity field of the fluid. This problem arises in separating emulsions Fang and Lai (1995), and in coating materials. In the latter case, powders are distributed on a surface and are heated with microwaves until they melt and smoothly coat the material. These applications motivate the use of both rigid-rigid and rigid-free boundary conditions. (Note that we do not consider interfacial deformations in the present study.) One of the main parameters of concern is that connected to incident power levels necessary to induce convective motion within the fluid layer.

Much work has been done in the area of convection driven by internal heat sources. The problem arises in geophysics and may be of importance in meteorology. Pellow and Southwell (1940) have studied the hydrodynamic stability of a fluid subject to a linear temperature profile. Sparrow, Goldstein and Johnson (1964) studied the effects of imposing a nonlinear temperature profile, due to a uniform volumetric heat source, on the stability of a fluid layer. The theory treats convective, insulated and fixed boundary conditions for the temperature. Roberts ([10],[11]), studied the convection patterns in a horizontal layer of fluid driven by a constant internal heat source. Using energy methods he constructs an iterative scheme to study the nonlinear stability characteristics of the fluid and resolves degeneracies left by linear stability theory. Watson (1968) studied the effects of introducing a uniform volumetric heat sink into an infinite horizontal fluid layer on the stability of the

fluid with fixed boundary conditions for the temperature. She further investigates the possibility of formation of double layers of convective cells for large values of the rate of heat loss by the stable sublayer of fluid at the top and concludes that such a formation does not occur if the temperature at the upper surface is less than that at the lower surface. Studies were performed for the rigid-rigid and free-free boundary cases. Yučel and Bayazitoğlu (1979) studied the effects of a nonuniform volumetric heat source on the stability of an infinite horizontal fluid layer. The source is induced by absorption of incident radiative energy penetrating into the fluid. They impose convective boundary conditions on the temperature and rigid-rigid boundary conditions on the fluid.

In studies focusing on hydrodynamic instabilities within the bulk fluid, the source in the heat equation was chosen either for mathematical convenience or as a simple model of radiative heat transfer. There are many applications in which a microwave source becomes the heat source for fluids such as water and ethanol and solids such as ceramics. This is owed to the fact that for these and other materials, microwaves can be an effective means for depositing energy rapidly and selectively within the material. The mechanisms for this deposition are ohmic and dipolar heating (see Von Hippel (1954), Ramo (1984), Feynman (1964)). The use of microwaves in the processing of materials, ie. heating, sintering, melting, is an active area of research. A study of microwave heating a cylindrical vessel of fluid with a free surface has been carried out by Stuerga and Lallemant (1993a,b), (1994), and Stuerga, Lallemant and Steichen-Sanfeld (1994). Experiments are presented to investigate microwave heating of a confined fluid under reduced pressure (free surface) and make conclusions about boiling, superheating and explosions occurring in a fluid heated with microwaves. Their work further suggests the ability to control the shape of the spatial thermal profile within the subject fluid through microwave irradiation. Stuerga, Lallemant and Zahreddine (1993) studied the interaction of

microwaves with water. This study gives evidence that thermal runaway can occur in water at appropriate microwave power levels. This is owed to the temperature dependence of the complex permittivity of water which can give rise to resonance of the electric field within this media and, hence, can give rise to bistable solutions for steady-state temperatures. M. Nachman and G. Turgeon (1984) studied the interaction of microwaves in multilayered material. Specifically, they studied the heating patterns that evolve within a three layered material and investigated the ability to preferentially heat a specific layer by introducing a flat reflector to create standing waves within the media.

In chapter 2 we consider in detail the microwave interaction with a fluid and the induced source term. Specifically, we see that changing the impinging wave frequency or the slab thickness alters that position where the basic temperature profile attains its maximum value within the fluid medium. We conduct a study of the hydrodynamic stability of a fluid layer heated with a microwave source. We make the assumption that the dielectric attributes of the subject material are independent of temperature. The unperturbed solutions are found and the linear stability of these basic solutions is investigated. The analysis suggests minimum power requirements necessary to generate convection within the fluid. We also find that this minimum power undulates as the thickness of the fluid slab or frequency of the microwave is altered.

In chapter 3 we develop a model which incorporates the temperature dependence of the complex permittivity of a material. The unperturbed solutions are found. We specifically focus on the steady-state temperature distributions. As will be seen, a thermal runaway phenomena can occur in certain fluids. We study the hydrodynamic stability of a fluid layer heated with a microwave source. It will be shown that the power levels needed to achieve an onset of convection within the fluid layer fall far below those necessary to cause thermal runaway within the fluid.

1.2 Applications of Microwaves in the Melting of Materials

As mentioned in the first part of our introduction, microwaves have potential applications involving the melting of solid materials such as in welding processes, removal/application of materials to/from surfaces and thawing frozen foods.

In studying such processes it is important to develop an understanding of the mechanisms describing the interaction of the microwave source with materials, as well as an understanding of the mechanisms involved in phase-change front formation and propagation. In applications such as the coating application mentioned previously a change of phase is involved in melting the solid to coat a surface. It is desirable to understand this melting process in order that it can be carried out in an efficient manner. (i.e. minimal expenditure of power is involved or a faster turnaround time is achieved). The use of microwaves in melting, may be useful in such applications as coating application/removal in that they provide a more uniform heating of many materials than do conventional heating sources. For many materials, microwaves may significantly reduce the likelihood of surface damage in the coating removal process. For example, in the removal of paint from wooden surfaces, the surface is less likely to be scorched if microwaves are used than if a conventional heating gun is used.

Many studies both theoretical and experimental have been made in the area of phase front propagation (see B. A. Boley (1961), I. Crank (1957), S. J Citron (1960) and others). One underlying assumption in many of these works is the latent heat balance (Stefan) condition along with a Dirichlet condition on the temperature imposed at the melting front. For a more comprehensive investigation of Stefan problems see Hill and Dewynne (1987), Crank (1984) and Rubinstein (1971). In short, the Stefan condition states that the melting front velocity is directly proportional to the difference in the energy fluxes on both sides of the melting front. In many of these studies the source/sink is imposed through the boundary. Other works by Crank (1984) deal with moving fronts induced by volumetric sources using enthalpy,

front fixing and other methods. Goodman (1958) approximated the propagation of a melting front by assuming a polynomial representation of the temperature in the liquid region and using a heat balance integral to construct a governing ordinary differential equation for the melting front. Huang and Wang (1994) investigated the propagation of a freezing front during metal casting with mold. They employ inverse methods to deduce a suitable boundary condition at the mold/casting interface and, with this estimated boundary condition, implement the enthalpy method to deduce the trajectory of the melting front. Sethian and Strain (1991) present an efficient algorithm for predicting crystal growth and dendritic solidification in supercooled media.

In chapter 4 we investigate the melting of dielectric solids using microwaves. We will treat the one-dimensional case. Specifically, we investigate the trajectory of the melting front in time and raise issues regarding feedback control on the power source. The model will incorporate Maxwell's equations along with an energy equation for both the liquid and solid regions. As we will see, there is a strong coupling between the melting front position, the electric field strengths of the liquid and solid regions and the temperature field of the liquid region. The Stefan condition is employed to model the movement of the melting front. Having posed the full mathematical model, the dynamics and steady states of the system are investigated.

CHAPTER 2

HYDRODYNAMIC STABILITY OF A FLUID LAYER: CONSTANT DIELECTRIC PERMITTIVITY CASE

2.1 The Model

We consider a viscous incompressible fluid of constant thermal conductivity k_t and viscosity μ, bounded between two infinite parallel plates a distance d apart. The initial temperature of the fluid, θ_0, is assumed to be the same as that of the surrounding space, and the corresponding initial fluid density is denoted by ρ_0. For simplicity, the bounding plates are taken to be transparent to the impinging microwave field. The geometry is shown schematically in Figure 1.

The equations governing this microwave heating problem are the time dependent Maxwell's equations for a moving medium, the energy equation, and the Navier-Stokes equations. In our model we assume that the fluid velocities generated are much smaller than the speed of light. Then the relativistic correction terms to the electromagnetic equations are negligible and Maxwell's equations reduce to their standard form in a stationary medium. The second assumption we make is the charge neutrality of the fluid. Thus, the Lorentz force in the momentum equation for the fluid is absent. Finally, we assume that the time required for the fluid or heat to diffuse a wavelength is much larger than a microwave period. The later is $O(10^{-10})$ seconds for commercial generators. This last assumption allows us to average all the governing equations over a microwave period (see appendix A). The resulting equations are a time harmonic version of Maxwell's equations and the time dependent Navier-Stokes and heat equations. The later contains the averaged microwave source term.

Within this framework, we assume that a plane time-harmonic electromagnetic wave of frequency ω impinges normally upon the fluid layer which fills the region $0 < z' < d$. A portion of this wave scatters from the interface $z' = d$, a portion

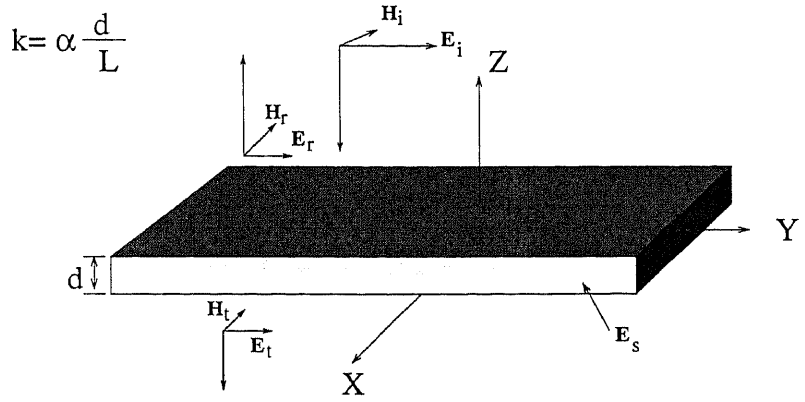

L = electromagnetic wave length

Figure 2.1 The geometry of the hydrodynamic problem.

penetrates the layer and heats the fluid, and the remaining portion is transmitted through the interface $z' = 0$. In the free space regions $z' > d$ and $z' < 0$, the electric field is given by the real parts of

$$\mathbf{E} = E_0 \left[e^{-i(k'z'+\omega t')} + \gamma e^{i(k'z'-\omega t')} \right] \mathbf{x}, \qquad z' > d, \tag{2.1}$$

$$\mathbf{E} = E_0 T e^{-i(k'z'+\omega t')} \mathbf{x}, \qquad z' < 0, \tag{2.2}$$

respectively, where E_0 is the strength of the incident field, $k' = \omega/c$, c is the speed of light in free space, T is the transmission coefficient, and γ is the reflection coefficient. Both T and γ are to be determined.

The electric field which penetrates the fluid and interacts with it is given by the real part of $\mathbf{E} = [E_2'(z')exp(-i\omega t')]]\mathbf{x}$, where E_2 satisfies

$$\frac{d^2 E_2'}{dz'^2} + k_1'^2 \left[1 + i\frac{\sigma_0}{\omega \epsilon_1} \right] E_2' = 0, \qquad 0 < z' < d, \tag{2.3}$$

In this equation $k_1' = (\omega/c)\sqrt{\epsilon_r}$, ϵ_0 is the permittivity of free space, ϵ_1 is the permittivity of the fluid and $\epsilon_r = \epsilon_1/\epsilon_0$ is the relative permittivity. If the fluid is purely dipolar, then σ_0 is the imaginary part of the dielectric constant. On the other hand, if the fluid is dipolar with conductive losses, then σ_0 is the effective conductivity, Kriegsmann (1993). In either case $\xi = \frac{\sigma_0}{\omega\epsilon_1}$ is a measure of how much power from the incoming wave is absorbed by the fluid; see Hippel (1954), Ramo, Whinnery and Van Duzer (1984). Implicit in the definition of k_1' is our assumption that the fluid is non-magnetic. We also assume here that all the electrical parameters, just defined, are independent of temperature.

From the continuity of the tangential electric and magnetic fields at $z' = d$ and $z' = 0$, we deduce that E_2 and its derivative are continuous there Ramo et al. (1984) (see section 3.14), Kriegsmann (1992). Combining this fact with (2.1-2.2) and eliminating T and γ, we find that E_2 satisfies the boundary conditions

$$\frac{dE_2'}{dz'} + ik'E_2' = 0, \qquad z' = 0, \tag{2.4}$$

$$\frac{dE_2'}{dz'} - ik'E_2' = -2ik'E_o e^{-ik'}, \qquad z' = d, \tag{2.5}$$

Equations (2.3-2.5) fully determine the electric field within the fluid and outside the fluid.

The electric field described above acts as a source of energy that heats the fluid. The fluid equations to be solved consist of the Navier-Stokes equations for heat conducting fluids coupled to a temperature equation which includes an energy supply due to the electric field. Denote dimensional fluid velocities, temperature and pressure by $\mathbf{u}' = (u_1', u_2', u_3')$, θ' and P' respectively. Making the usual Boussinesq approximation, $\rho = \rho_0(1 - \alpha(\theta' - \theta_0))$ where α is the coefficient of thermal expansion of the fluid, (see Drazin & Reid (1981)) leads to the following system:

$$\rho_o \frac{Du_i'}{Dt} = -g\rho_o(1 - \alpha(\theta' - \theta_o))\delta_{i3} - \nabla P' + \mu\triangle u_i', \tag{2.6}$$

$$\nabla \cdot \mathbf{u}' = 0, \tag{2.7}$$

$$\rho_o c_p \frac{D\theta'}{Dt} = \frac{\partial}{\partial x'_j}(k_t \frac{\partial \theta'}{\partial x'_j}) + \frac{\sigma_o}{2}|E'_2|^2, \tag{2.8}$$

where $\mathbf{x}' = (x', y', z')$ and $\triangle = \frac{\partial^2}{\partial x'^2} + \frac{\partial^2}{\partial y'^2} + \frac{\partial^2}{\partial z'^2}$. The boundary conditions are those of no slip for fluid velocities at the solid walls

$$u'_1 = u'_2 = u'_3 = 0, \qquad z = 0, d, \tag{2.9}$$

In the case of a free upper surface the boundary condition at $z = d$ becomes

$$\frac{\partial u'_1}{\partial y'} + \frac{\partial u'_3}{\partial x'} = \frac{\partial u'_2}{\partial x'} + \frac{\partial u'_3}{\partial y'} = 0, \quad u'_3 = 0, \qquad z = d, \tag{2.10}$$

and convective conditions for the temperature at the walls

$$k_t \frac{\partial \theta'}{\partial z} = h(\theta' - \theta_o), \qquad z = 0, \tag{2.11}$$

$$k_t \frac{\partial \theta'}{\partial z} = -h(\theta' - \theta_o), \qquad z = d, \tag{2.12}$$

In equations (2.6-2.12) above g is the acceleration due to gravity, c_p is the specific heat of the fluid and h is the heat transfer coefficient measuring loss of heat due to convective cooling. The source term in (2.8) is due to the microwave interaction with the fluid.

The governing equations are made dimensionless by scaling distances with the slab thickness d, time by the diffusive time scale d^2/κ where $\kappa = k_t/(\rho_0 c_p)$ and the electric field by the incident amplitude E_0. New variables are introduced as

$$\begin{aligned} &\mathbf{x} = \mathbf{x}'/d, \quad t = \kappa t'/(d^2), \quad \mathbf{u} = d\mathbf{u}'/\kappa \\ &P = d^2/(\kappa^2 \rho_o) P', \quad \theta = (-1 + \frac{\theta'}{\theta_o})/\chi, \end{aligned} \tag{2.13}$$

New electric field variables are introduced as

$$E = E'/(e^{-ik'} E_0), \quad k = k'd, \quad k_1 = k'_1 d, \tag{2.14}$$

Substitution of (2.13),(2.14) into (2.3-2.5) and (2.6-2.8) gives the dimensionless system given below. The nondimensional groups which enter into the dynamics

are the Rayleigh number, R, the Prandtl number, Pr, the Biot number, β, and a nondimensional measure of the incident microwave power denoted by χ. These groups are given by:

$$R = (\alpha g d^3 \theta_o)/(\kappa\nu), \quad Pr = \nu/\kappa, \quad \beta = hd/k_t, \quad \chi = \sigma_o |E_o|^2 d^2/(2k_t\theta_o), \tag{2.15}$$

These scalings produce the nondimensional system:

$$\frac{d^2E}{dz^2} + {k_1}^2(1 + i\xi)E = 0, \tag{2.16}$$

$$\nabla \cdot \mathbf{u} = 0, \tag{2.17}$$

$$\frac{D\mathbf{u}}{Dt} = -\nabla(P + gzd^3/\kappa^2) - R\chi Pr\theta\mathbf{k} + Pr\triangle\mathbf{u}, \tag{2.18}$$

$$\frac{D\theta}{Dt} = \triangle\theta + |E|^2, \tag{2.19}$$

$$\frac{dE}{dz} + ikE = 0, \qquad z = 0, \tag{2.20}$$

$$\frac{dE}{dz} - ikE = -2ik, \qquad z = 1, \tag{2.21}$$

$$\frac{\partial\theta}{\partial z} = \beta\theta, \qquad z = 0, \tag{2.22}$$

$$\frac{\partial\theta}{\partial z} = -\beta\theta, \qquad z = 1, \tag{2.23}$$

Rigid − rigid $\qquad u_1 = u_2 = u_3 = 0, \qquad z = 0, 1,$ (2.24)

Free upper surface $\qquad \dfrac{\partial u_1}{\partial y} + \dfrac{\partial u_3}{\partial x} = \dfrac{\partial u_2}{\partial x} + \dfrac{\partial u_3}{\partial y} = 0, \quad u_3 = 0, \qquad z = 1,$ (2.25)

where $\mathbf{k}$ is the unit vector in the z direction. It should be noted that in the basic state (ie. $\mathbf{u} = \mathbf{0}$), the governing equations for the temperature θ and the electric field E are independent of the flow and are not affected by the Boussinesq approximation.

2.2 Basic States

The base flow velocities are $\mathbf{u} = \mathbf{0}$ and equation (2.18) gives the corresponding pressure distribution. Since equations (2.16) and (2.19) are decoupled, as long as

ξ is independent of temperature, we can explicitly determine the electric field and hence the temperature. The solution for the electric field is given by:

$$\overline{E} = \frac{2ik[\Gamma\cos(\Gamma(1-z)) - ik\sin(\Gamma(1-z))]}{\sin(\Gamma)(\Gamma^2+k^2) + 2ik\Gamma\cos(\Gamma)}, \tag{2.26}$$

where $\Gamma = k_1\sqrt{(1+i\xi)}$. The corresponding temperature field is obtained by substituting (2.26) into (2.19), integrating with respect to z, and applying 2.22 and 2.23; the result is

$$\overline{\theta}(z) = -\int_0^z |\bar{E}|^2(z-s)ds + (\beta z+1)\frac{1}{\beta(2+\beta)}\int_0^1 |\bar{E}|^2(1+\beta(1-s))ds, \tag{2.27}$$

Note that the electric field (2.26) depends on k (this parameter is the ratio of the slab thickness to the microwave length) and the parameter ξ through the parameter Γ. In Figures 2.2a-d we give typical undisturbed temperature distributions within the slab for different microwave frequencies k for fixed Γ and unit Biot number, $\beta = 1$. (We mention that these temperature profiles are those needed to achieve an onset of instability within fluid, as is explained in Section 3.) As can be seen from the profiles in figure 2.2, the position of maximum temperature within the slab is a complicated function of k - in fact it is found to oscillate with k as we will see later.

2.2.1 A Limiting Case $k \to 0$ (Low Frequency)

The case of long microwaves, $k << 1$, can be analyzed asymptotically. Assuming that ϵ_r is of order one we can expand in powers of k where $k_1 = \epsilon_r k$ to approximate the electric field as $E = E_o + E_1 k + E_2 k^2 \ldots$. Substituting this into (2.16) and utilizing the boundary conditions (2.20),(2.21) yields the following system:

$$\frac{d^2(E_o + kE_1 + \cdots)}{dz^2} + \epsilon_r k^2(1+i\xi)(E_o + kE_1 + \cdots) = 0, \tag{2.28}$$

$$\frac{d(E_o + kE_1 + \cdots)}{dz} - ik(E_o + kE_1 + \cdots) = -2ik, \quad z = 1, \tag{2.29}$$

$$\frac{d(E_o + kE_1 + \cdots)}{dz} + ik(E_o + kE_1 + \cdots) = 0, \quad z = 0, \tag{2.30}$$

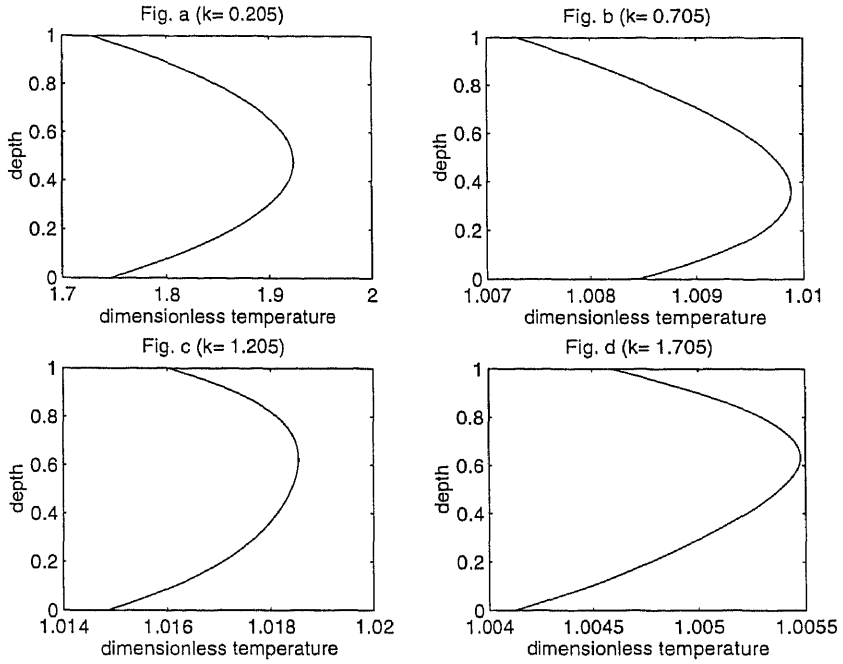

Figure 2.2 Typical undisturbed temperature profiles; the physical parameters are $\beta = 1$; $\epsilon_r = 2.54$; $\xi = .25$.

The leading order system is:

$$\frac{d^2E_o}{dz^2} = 0, \tag{2.31}$$

$$\frac{dE_o}{dz} = 0, \quad z = 1, \tag{2.32}$$

$$\frac{dE_o}{dz} = 0, \quad z = 0, \tag{2.33}$$

Solving this system we find $E_o = B$ where B is any constant. To solve for B we must look to the next order system:

$$\frac{d^2E_1}{dz^2} = 0, \tag{2.34}$$

$$\frac{dE_1}{dz} - ikE_o = -2ik, \quad z = 1, \tag{2.35}$$

$$\frac{dE_1}{dz} + ikE_o = 0, \quad z = 0, \tag{2.36}$$

Solving for E_1, we find $E_1 = Cz + D$ so $\frac{dE_1}{dz} = C$. We now utilize the boundary conditions to construct an algebraic system that lets us solve for B:

$$C - ikB = -2ik, \tag{2.37}$$

$$C + ikB = 0, \tag{2.38}$$

Hence $B = E_o = 1$ so $E = 1$ to leading order. Substituting this expression for E into (2.27), we obtain the following:

$$\bar{\theta}(z) = -z^2/2 + z/2 + 1/(2\beta), \tag{2.39}$$

This is the familiar parabolic temperature distribution that would be obtained from constant volumetric source heating (see Introduction).

2.3 Linear Stability

The linear stability of the undisturbed states described above, can be analyzed by adding small perturbations $\mathbf{u}'$, θ', P' and E' and linearizing (2.16-2.25) with respect to primed quantities to obtain:

$$\nabla \cdot \mathbf{u}' = 0, \tag{2.40}$$

$$\frac{\partial \mathbf{u}'}{\partial t} = -\nabla P' - R\chi Pr\theta' \mathbf{k} + Pr\triangle \mathbf{u}', \tag{2.41}$$

$$\frac{\partial \theta'}{\partial t} + \frac{d\bar{\theta}}{dz} w' = \triangle \theta', \tag{2.42}$$

Taking the curl of (2.41) twice, we obtain the following equation involving the vertical velocity component of the fluid and the temperature:

$$\frac{\partial \triangle w'}{\partial t} = R\chi Pr \triangle_1 \theta' + Pr\triangle^2 w', \tag{2.43}$$

where $\triangle_1 = \frac{\partial^2}{\partial x^2} + \frac{\partial^2}{\partial y^2}$. This equation along with (2.42) will be used to determine the stability of the system. Note that with the eigenfunctions w' and θ' known the continuity equation (2.40) along with (2.41) yields the velocity components u' and v' as well as the perturbation pressure P'.

Equations (2.42) and (2.43) comprise a coupled system of PDEs which can be analyzed by introducing the normal modes

$$\theta' = \Theta(z) f(x,y) e^{\sigma t}, \qquad w = W(z) f(x,y) e^{\sigma t}, \tag{2.44}$$

into (2.42) and (2.43). For example, the energy equation (2.42) becomes

$$\left[\sigma + \frac{\overline{\theta}_z W}{\Theta} - \frac{D^2\Theta}{\Theta}\right] = \frac{\triangle_1 f}{f},$$

which on introduction of a separation constant a^2, yields the Helmholtz equation $\triangle_1 f + a^2 f = 0$ for the horizontal dependence of the temperature eigenfunction. Proceeding as above and using the momentum equation (2.43) also, yields the following eigenvalue problem depending on the wavenumber a which arises from the Helmholtz equation and which measures the wavelength of linear perturbations:

$$(D^2 - a^2)(Pr(D^2 - a^2) - \sigma)W - a^2 R\chi Pr\Theta = 0, \tag{2.45}$$

$$(D^2 - a^2 - \sigma)\Theta - WD\overline{\theta} = 0, \tag{2.46}$$

$$\underline{\text{Rigid} - \text{rigid}} \quad W = DW = 0, \qquad z = 0, 1, \tag{2.47}$$

$$\underline{\text{Rigid} - \text{free}} \quad W = D^2 W = 0, \qquad z = 1, \tag{2.48}$$

$$\frac{d\Theta}{dz} = \beta\Theta, \qquad z = 0, \tag{2.49}$$

$$\frac{d\Theta}{dz} = -\beta\Theta, \qquad z = 1, \tag{2.50}$$

Marginal stability of the above system is given by $\sigma = 0$. Although exchange of stabilities has not been proven in the present problem (the difficulty arises due to the fact that $\frac{d\overline{\theta}}{dz}$ is non-constant in the slab), it is strongly suggested numerically.

2.4 Numerical Solutions

Due to the complicated form of the background temperature variations (see (2.26) and (2.27)) a closed form solution of the eigenvalue problem has not proven possible, and so we proceed numerically. However, some limiting cases are considered later. The problem was solved numerically using a Matlab ODE solver (ode45) in conjunction with a shooting method. Before proceeding with a description of our numerical results, we make some comparisons with other related investigations.

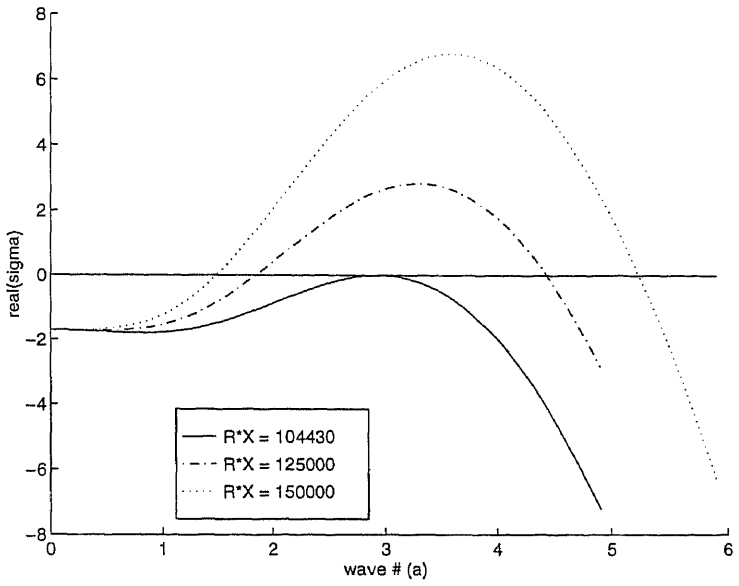

Figure 2.3 Growth rate curves, rigid-rigid case; $\beta = 1$; $k = 1$; $\epsilon_r = 2.54$; $Pr = 17$; $\xi = .25$.

Roberts (1967), has considered convection problems with uniform internal heat sources (i.e. producing parabolic undisturbed temperature profiles), with isothermal boundary conditions on the upper face and an insulating condition on the lower face - these conditions translate, in our notation, to $\overline{\theta} = 0$ at $z = 1$, and $\frac{d\overline{\theta}}{dz} = 0$ at $z = 0$ and similar expressions for the perturbation. This scenario can be recovered from our system by (i) letting the Biot number $\beta \to \infty$ on the upper face (this gives $\overline{\theta} = 0$ at $z = 1$ to leading order),(ii) letting $\beta \to 0$ at $z = 0$ (giving $\frac{d\overline{\theta}}{dz} = 0$ at the lower face), and, (iii) letting $k \to 0$ to obtain the background temperature distribution given by (2.39). Our code reproduces the neutral stability results of Roberts noting that his Rayleigh number, in our notation, is given by $R\chi$.

An additional test of our numerical procedure is possible in the limiting case of $\beta \to 0$ on both the upper and lower faces, along with $k \to 0$ to produce uniform volumetric heating. This is a special case addressed in the stability study of Yučel and Bayazitoğlu where the attenuation coefficient is zero. Our results are in complete agreement with theirs. In particular we obtain the same critical value of the Rayleigh number $R\chi = 37328$.

2.4.1 A Limiting Case (Low Wave Number Perturbative Modes)

It is seen from Figure 2.3 that in the long wave limit $a \to 0$, the flow is stable with a decay rate independent of $R\chi$. The numerical value found for the set of physical parameters of Figure 2.3, is -1.707. This result can be confirmed analytically by an asymptotic expansion for small a. In the limit $a \to 0$, the system (2.45-2.50) becomes, to leading order,

$$(D^4 - \frac{\sigma}{Pr}D^2)W = 0, \tag{2.51}$$

$$(D^2 - \sigma)\Theta - D\tilde{\theta}W = 0, \tag{2.52}$$

$$W = DW = 0, \qquad z = 0, 1, \tag{2.53}$$

$$D\Theta = \beta\Theta, \qquad z = 0, \tag{2.54}$$

$$D\Theta = -\beta\Theta, \qquad z = 1, \tag{2.55}$$

Multiplying (2.51) by W^* and (2.52) by Θ^* where stars denote the complex conjugates, and integrating by parts we arrive at the following equations:

$$\int_0^1 |D^2W|^2 dz + \sigma \int_0^1 |DW|^2 dz = 0, \tag{2.56}$$

$$-\int_0^1 |D\Theta|^2 dz - \sigma \int_0^1 |\Theta|^2 dz + \int_0^1 D(\tilde{\theta})\Theta^* W dz = 0, \tag{2.57}$$

First we use (2.56) and (2.57) to show that σ must be real. If W is non-zero, then (2.56) is sufficient to determine that σ is real. If $W(z) = 0$, σ is seen to be real from (2.57). In addition the expressions (2.56) and (2.57) show that if $\sigma = 0$ then both $W(z)$ and $\Theta(z)$ are zero resulting in a trivial solution.

It has been found numerically that the W eigenfunction tends to zero as a decreases, while the corresponding Θ eigenfunction is non-trivial. This behavior is illustrated in Figures 2.4a,b where $W(z)$ and $\Theta(z)$ are plotted for different decreasing wavenumbers and $R\chi = 125000$, the other parameters being those of Figure 2.3.

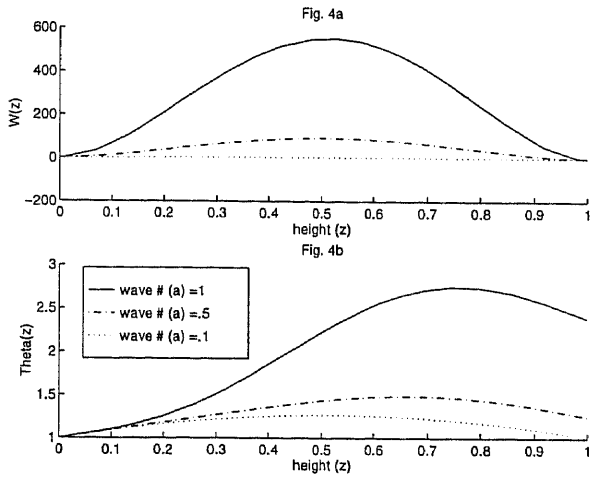

Figure 2.4 Eigenfunctions $W(z)$ (top) and $\Theta(z)$ (bottom); $\beta = 1; k = 1; \epsilon_r = 2.54$; $Pr = 17$; $\xi = .25$.

Writing $W(z) = 0 + \ldots$, then, the system (2.51-2.55) is decoupled and can be solved exactly for Θ to obtain the following eigen relation for σ:

$$\tan(\sqrt{-\sigma})(\beta^2/\sqrt{-\sigma} - \sqrt{-\sigma}) + 2\beta = 0, \tag{2.58}$$

The eigenrelation (2.58) was solved numerically to determine the largest eigenvalue for σ to be -1.70, in complete agreement with the numerical solutions presented in Figure 2.3. Note that this value is independent of $R\chi$ as is demonstrated in Figure 2.3.

2.4.2 A Limiting Case (Stability of Modes for Large Critical Power Levels)

As can be seen from Figure 2.6, an unstable mode exists if the (modified) Rayleigh number is large enough. In fact, asymptotic methods can be used to analyze the most unstable mode as $R\chi \to \infty$ as presented next. Consider equations (2.45)-(2.46) with $R\chi$ asymptotically large and the wavenumber a of order one. The leading order balance leads to an inviscid system away from the walls. More formally, a balance of terms in (2.45)-(2.46) leads to the expansions

$$W = (R\chi)^{1/2} W_0 + \ldots, \quad \Theta = \Theta_0 + \ldots, \quad \sigma = (R\chi)^{1/2}\sigma_0, \tag{2.59}$$

where $\sigma_0(a)$ is the scaled eigenvalue to be found. These expansions lead to the inviscid leading order eigenvalue problem (after elimination of Θ_0 between (2.45) and (2.46)):

$$\sigma_0^2(D^2 - a^2)W_0 - a^2\frac{d\overline{\theta}}{dz}W_0 = 0,$$
$$W_0 = 0, \quad \text{on} \quad z = 0, 1, \tag{2.60}$$

We note that in the case of a parabolic basic temperature profile $\overline{\theta}$, the system (2.60) is analogous to the stability of Couette flow in the gap between concentric cylinders at large Taylor numbers (see Drazin & Reid (1981)), which can be solved in terms of Airy functions; in that special case it is found that σ_0 is bounded above by a constant, c_0 say, and $\sigma_0 \to c_0$ as $a \to \infty$. The most unstable mode is for short waves and viscous boundary layers are required to reduce this to zero as the right hand neutral branch of the stability curves is approached (see Figure 2.6, for instance).

In the case of general wavelength microwaves the eigenvalues must be computed numerically for different values of a. Similar trends as in the parabolic profile case are found. Typical results of solutions of (2.60) are shown in Figure 2.5; the eigenfunction $W_0(z)$ is shown for wavenumbers $a = 1, 100, 1000$ for the physical parameters indicated. It is seen that as a increases the mode is concentrated near $z = 1$ and is zero away from it. This can be quantified by constructing WKB solutions of (2.60) as $a \to \infty$; a turning point exists in these solutions near $z = 1$ and solutions valid below and above the turning point can be constructed by standard matching methods. The matching provides an upper bound on the leading order eigenvalue σ_0,found to be

$$\sigma_0^2 \to -\min\left(\frac{\mathrm{d}\overline{\theta}}{\mathrm{dz}}\right), \quad 0 \leq \mathrm{z} \leq 1.$$

For the parameters given in Figure 2.5, the result is $\sigma_0^2 \to .1277$ as $a \to \infty$. See Appendix C.

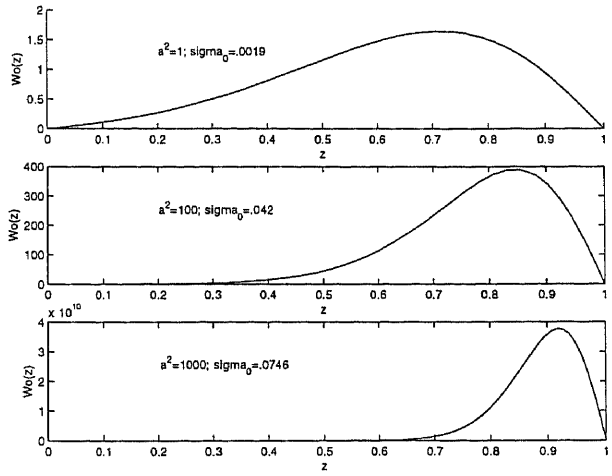

Figure 2.5 Asymptotic eigenfunctions at large $R\chi$; $\beta = 1$; $k = 1$; $\epsilon_r = 2.54$; $\xi = .25$.

2.5 Results

Stability characteristics were obtained by fixing the physical parameters including the microwave power (in non-dimensional terms this is χ) which in turn fixes the power Rayleigh number $R\chi$. For different wavenumbers a, the eigenvalue σ, which is complex in general, was computed by iteration. Our numerical results produce real values of σ alone, indicating that there is no propagation of disturbances down the slab. In addition these results suggest that neutral curves can be traced by specifying $\sigma = 0$. A typical set of results is given in Figure 2.3 for different power Rayleigh numbers and physical parameters (shown on the Figure) corresponding to ethyl alcohol. As can be seen, larger values of $R\chi$ support a band of unstable modes which narrows as the modified Rayleigh number decreases - see the curves corresponding to $R\chi = 150000$ and 125000 respectively. As the modified Rayleigh number is decreased further, it reaches a critical value below which the flow is linearly stable to all wavelengths. The critical value for the set of parameters of Figure 2.3 is found to be 104430 and the corresponding variation of σ with wavenumber is also given. It can be concluded, therefore, that the qualitative effect of increasing the microwave power is an enhancement of the instability.

Next we use typical stability plots, as in Figure 2.3, to present neutral curves which have $\sigma = 0$. For a fixed $R\chi$ it is seen that there are at most two values of the wavenumber where the flow is neutrally stable, and below a critical value of $R\chi$, denoted by $R\chi_c$, the flow becomes linearly stable to all wave numbers. Neutral curves of $R\chi$ against a for different Biot numbers (other parameters being fixed) are considered first. In Figure 2.6 we show neutral curves for $\beta = 0.01$ and 1.0 when the non-dimensional parameter $k = 1.0$. The unstable and stable regions are located above and below the given neutral curve respectively. In fact each neutral curve provides a critical minimum point $(a_c, R\chi_c)$; flows corresponding to Rayleigh numbers below $R\chi_c$ are stable. The variation of $(a_c, R\chi_c)$ in parameter studies provides a lot of information about the stability characteristics and is considered later. Physically, β may be associated with the rate at which heat is convected away from the slab and hence an increase in the Biot number has a stabilizing effect on the system. That is, for a given value of $R\chi$ the window of unstable modes contributing to the disturbance in the fluid decreases. In the case of a free upper surface the marginal curve drops indicating that the fluid is more prone to become stable. These observations indicate that the more constrained a system, the greater its stability.

One main difference between background heating profiles produced by microwave radiation with those produced by constant volumetric heat sources, is that in the former case the height (z) where the background temperature is a maximum varies with k, whereas it is fixed at $z = 1/2$ when k tends to zero (see (2.39)). This has an important influence on the convection patterns that emerge since the point of maximum temperature separates regions of negative thermal gradients above and positive ones below. It can be expected, then, that in regions where the thermal gradient is positive the flow is stable and the resulting perturbation velocities are small. Convection patterns in the form of rolls should have centers which are displaced vertically upwards.

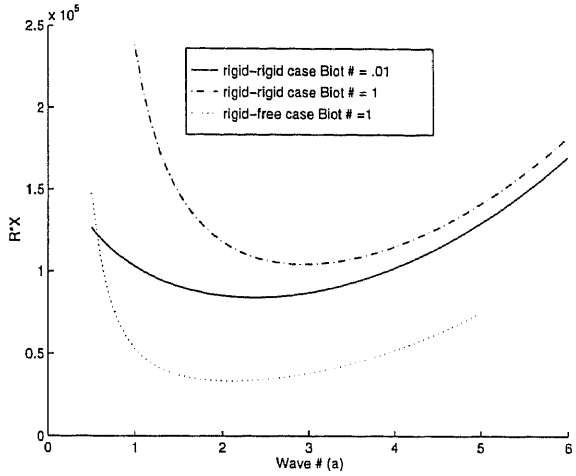

Figure 2.6 Neutral stability curves in the $R\chi$-a plane; $k = 1$; $\epsilon_r = 2.54$; ; $\xi = .25$.

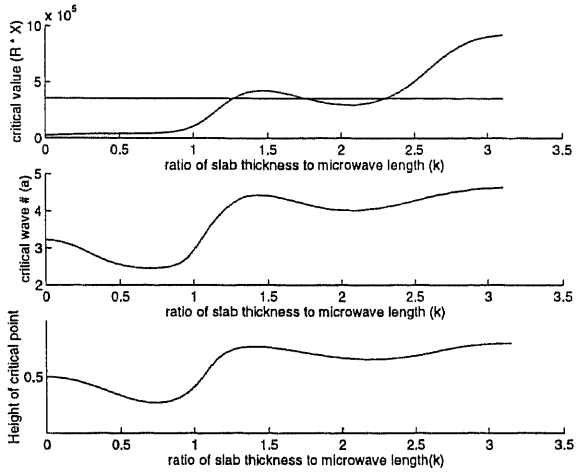

Figure 2.7 Neutral curves rigid-rigid case: $\beta = 1$; $\epsilon_r = 2.54$; $\xi = .25$.

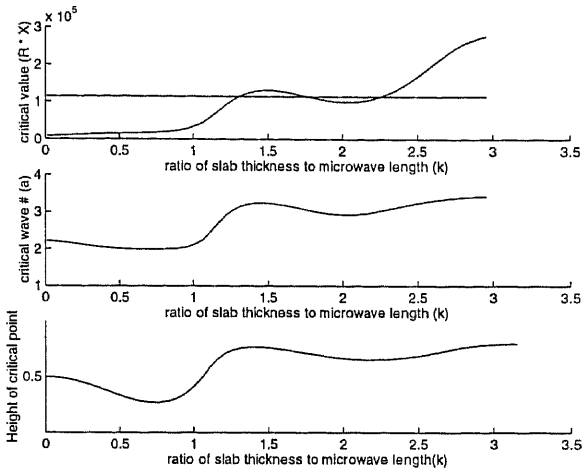

Figure 2.8 As in Figure 2.7 but rigid-free boundary conditions.

We now quantify these observations by presenting numerical solutions of the eigenvalue problem. Figure 2.7a gives the variation of the critical values of $R\chi_c$ with k, the ratio of slab thickness to microwave length. Figure 2.7b is a plot of the critical wavenumber a_c versus k, and Figure 2.7c presents the variation of the height where the background temperature achieves its maximum, z_{max} say, with k. The critical values for $R\chi$ are those values at which the onset of instability is achieved and exactly one perturbation mode corresponding to the critical wave number a_c becomes excited. It can be seen from these results that the variations with k of the three quantities plotted in Figure 2.7a-c are roughly in phase. This can be explained physically as follows: Consider Figure 2.7c first. A decrease in the height z_{max} implies that there is a larger unstable layer of fluid residing near the upper boundary. The lower stable region is almost stagnant (see later also). The size of convection cells is expected to scale with the size of the unstable layer, and so decreasing z_{max} increases the size of the cells which are proportional to $1/a_c$. This argument indicates that the variations of a_c and z_{max} with k should be roughly in phase, and this is supported by the numerical results. Figure 2.7a also indicates an in-phase behavior between $R\chi_c$ and z_{max}. This can be attributed to the fact that a decrease in z_{max} provides a larger unstable body of fluid to be convected, which could be achieved with a lower power

input, i.e. a lower $R\chi_c$. Again, the numerical results produce in-phase variations with the exception of small values of k. We note that the non-monotonic behavior in Figure 2.7a, for example, is capable of producing the same critical Rayleigh number for three different microwave lengths (see Figure). This mechanism can be used to obtain similar convection cell sizes for different values of k. Figures 2.8a-c show similar plots for a lower rigid and free upper boundary. The critical values of $R\chi$ are lower as might be expected since tangential slip is now permitted at the upper slab face and the system is less constrained. Finally, we observe that in both cases the overall trend of $R\chi_c$ with k is increasing. Since $R\chi$ scales with E_0^2, the power of the incident field, and k scales with the slab thickness d, this trend indicates that thicker fluid slabs require more power to become unstable. The local minimum at $k \sim 2$ occurs because the magnitude of the electric field deduced from Figure 2.7 has a maximum there. This is a resonance phenomenon. Thus, the strength of the incident field and the value of $R\chi_c$ required for the onset of an instability are reduced. Similarly, the local maximum at $k \sim 3$ occurs because the magnitude of the electric field is minimum. This is an anti-resonant behavior. Thus, the strength of the incident field and the value of $R\chi_c$ required for the onset of an instability are increased.

In closing this section we present a typical flow which shows convection cells at the onset of instability. Two values of k (.705, 1.355) are chosen, yielding a z_{max} less than $1/2$ and greater than $1/2$ respectively. The Biot number in both cases is one, and the material parameters are those for ethyl alcohol. Critical wavenumbers and Rayleigh numbers are obtained numerically as described earlier, and the convective cells shown in Figures 2.9-2.10 and were generated by choosing $f(x, y) = \cos(ax)$ and utilizing the computed eigenfunctions. Also shown on the figures are the corresponding background temperature profiles (note that these have been scaled up for illustrative reasons). The figures support our earlier observations of Figures 2.7a-c,

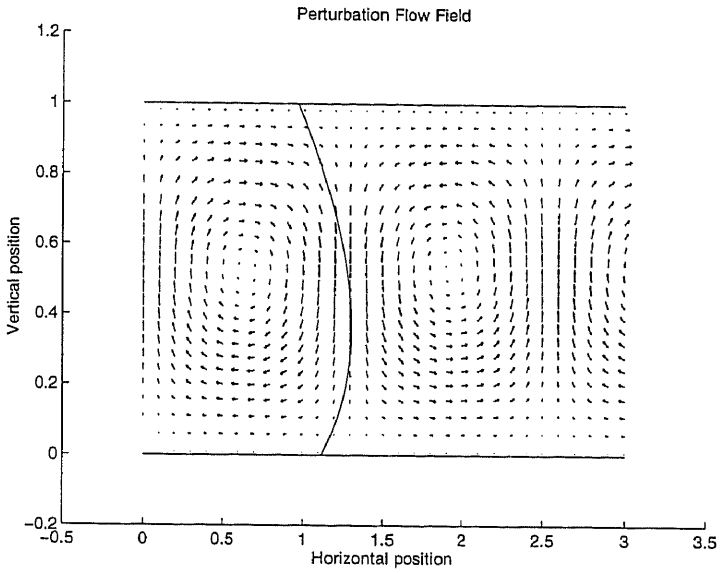

Figure 2.9 Perturbation flow field at onset; base temperature profile x 10 superimposed on flow field. $\beta = 1$; $k = .705$; $\epsilon_r = 2.54$; $\xi = .25$; critical wave number a_c =2.45.

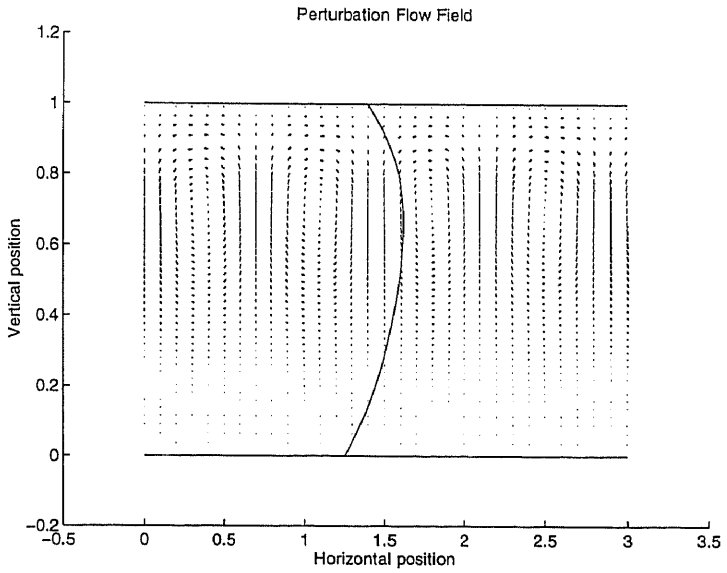

Figure 2.10 Perturbation flow field at onset; base temperature profile x 10 superimposed on flow field. $\beta = 1$; $k = 1.355$; $\epsilon_r = 2.54$; $\xi = .25$; critical wave number a_c =4.401.

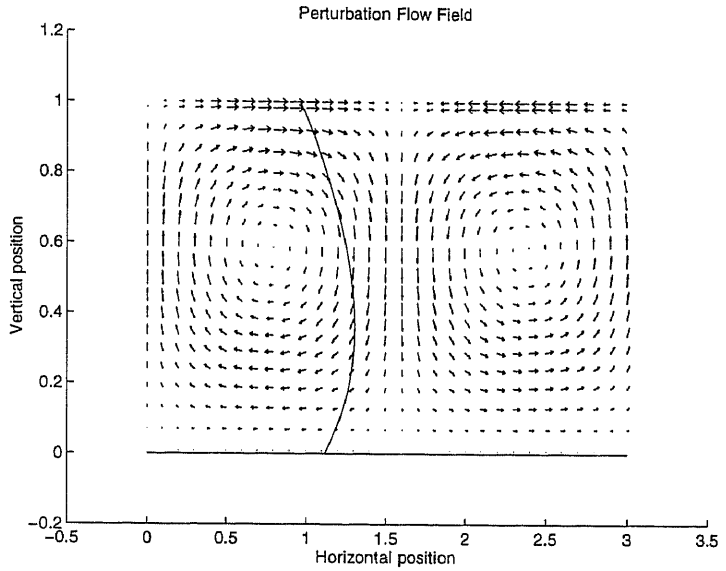

Figure 2.11 Perturbation flow field at onset; base temperature profile x 10 superimposed on flow field. $\beta = 1$; $k = .71$; $\epsilon_r = 2.54$; $\xi = .25$; critical wave number a_c =1.99.

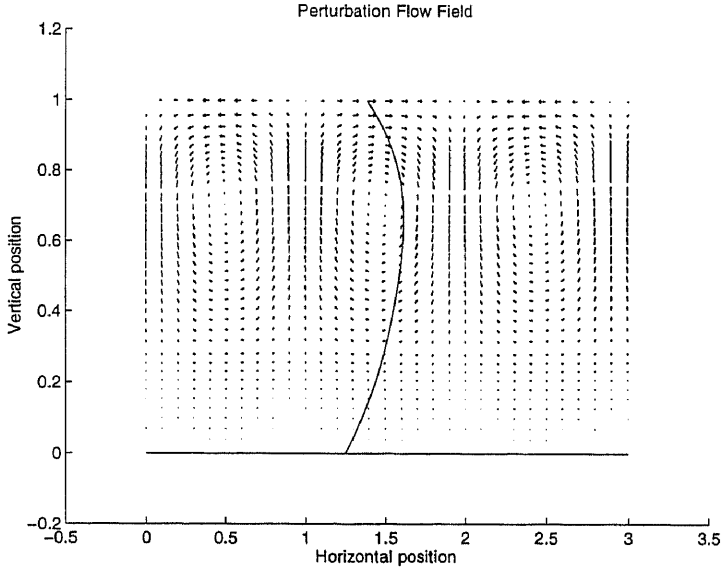

Figure 2.12 Perturbation flow field at onset; base temperature profile x 10 superimposed on flow field. $\beta = 1$; $k = 1.36$; $\epsilon_r = 2.54$; $\xi = .25$; critical wave number a_c =3.22.

and it is seen that the cell-size in Figure 2.9 is larger than that of Figure 2.10; in addition the cell centers lie above z_{max} and flow velocities below z_{max} (i.e. in the stable region) are smaller than those in the unstable region. Figures 2.11 and 2.12 show representative flows for the rigid-free boundary case. These graphs support the results of figures 2.8a-c.

2.6 Discussion

We have considered convective instabilities in fluids heated by microwaves. For constant electrical conductivities it has been found that the induced background temperature gradients produce convective cells when a critical Rayleigh number is exceeded. Microwave heating is equivalent to volumetric heating but the profiles produced are more complicated since they result from the power supplied by the non-uniform electric field within the slab. One common feature, however, is the presence of a temperature maximum at some height in the slab and consequently a region of stable fluid (cooled from below) and a region of unstable fluid (heated from below). An interesting feature of the microwave produced background temperatures, is that the position of maximum temperature can be varied by varying the microwave frequency; the variations are oscillatory with the non-dimensional parameter k (see earlier definition). It has been found numerically that critical Rayleigh numbers as well as critical wavenumbers are qualitatively in phase with these changes in background temperature. This implies that resulting convection cell sizes can be manipulated in a controlled manner by varying the microwave frequency.

We finally turn to some observations that may be useful for experimental investigations. Given a fluid (such as ethyl alcohol for instance), and the operating Biot number, we now illustrate how Figure 2.7 can be used to predict experimental parameters for onset of convection. Consider first a slab with fixed thickness d (we are assuming here that the width is much larger than the thickness). It is useful to

know the incident microwave power, P_{inc} say, required to produce instability. Using the non-dimensional groups (2.15) and the result $P_{inc} = q|E_0|^2$ where q is a material constant, we see that $R\chi$ is proportional to the incident power. With the slab thickness given, and for known operating microwave frequency, we can determine their ratio, k. Figure 2.7, then, provides a variation between the required P_{inc} with k. Similar conclusions can be drawn from fixing the microwave amplitude $|E_0|^2$ and the frequency, and using Figure 2.7 to deduce the thickness d required for onset.

Finally we consider possible weakly nonlinear developments and in particular the emergence of roll or hexagon cellular patterns. Of relevance is the work of Tveitereid and Palm (1976) who consider convection due to an internal heat source and with boundary conditions of fixed temperature at one wall the other wall being insulated. The basic profile is parabolic, then, and the linear stability problem is not self-adjoint. Due to this, it is shown that hexagons are the stable emerging patterns. It can be shown that a similar situation applies here; the analysis is standard and lengthy and is not included here.

CHAPTER 3

HYDRODYNAMIC STABILITY OF A FLUID LAYER: TEMPERATURE DEPENDENT COMPLEX PERMITTIVITY

3.1 The Model

The physical configuration is the same as for the constant conductivity case dealt with in Chapter 2. The fact that the dielectric attributes of the fluid are temperature dependent requires scalings of variables that are somewhat different from those given in the constant conductivity case. We consider a viscous incompressible fluid of constant thermal conductivity k_t and viscosity μ, bounded between two infinite parallel plates a distance d apart. The initial temperature of the fluid, θ_0, is assumed to be the same as the surrounding space, and the corresponding initial fluid density is denoted by ρ_0. For simplicity, the bounding plates are taken to be transparent to the impinging microwave field. The geometry is shown schematically in Figure 2.1.

As was argued in Chapter 2 we can average all of the governing equations over a microwave period. The resulting equations are a time harmonic version of Maxwell's equations and the time dependent Navier-Stokes and heat equations. The latter contains the averaged microwave source term (see appendix A).

Within this framework, we assume that a plane, time harmonic electromagnetic wave of frequency ω and strength E_o impinges normally upon the fluid layer which fills the region $0 < z < 1$. A portion of this wave scatters from the interface $z = 1$, a portion penetrates the layer and heats the fluid, and the remaining portion is transmitted through the interface $z = 0$. Let $\mathbf{E}_I$ denote electric field in the region above the slab ($z > d$), $\mathbf{E}_{II}$ denote electric field within the slab ($0 < z < d$) and $\mathbf{E}_{III}$ denote electric field below the slab ($z < 0$).

The electric field generated within the slab acts as a source of energy that heats the fluid. The fluid equations to be solved consist of the Navier-Stokes equations for heat conducting fluids coupled to a temperature equation which includes an energy

supply due to the electric field. This electric field is coupled to the heat equation and can not be solved for exactly. Denote dimensional fluid velocities, temperature and pressure by $\mathbf{u}' = (u_1', u_2', u_3')$, θ' and P' respectively. Making the usual Boussinesq approximation, $\rho = \rho_0(1-\alpha(\theta'-\theta_0))$ where α is the coefficient of thermal expansion of the fluid, (see Drazin & Reid (1981)) leads to the following system:

$$\triangle \mathbf{E}'_{II} - \nabla(\nabla \cdot \mathbf{E}'_{II}) + k'^2 \left[\epsilon'(\theta') + i\epsilon''(\theta')\right] \mathbf{E}'_{II} = 0, \tag{3.1}$$

$$\rho_o \frac{Du_i'}{Dt} = -g\rho_o(1-\alpha(\theta'-\theta_o))\delta_{i3} - \nabla P' + \mu \triangle u_i', \tag{3.2}$$

$$\nabla \cdot \mathbf{u}' = 0, \tag{3.3}$$

$$\rho_o c_p \frac{D\theta'}{Dt} = \frac{\partial}{\partial x_j'}(k_t \frac{\partial \theta'}{\partial x_j'}) + \frac{\omega \epsilon''(\theta')}{2} |\mathbf{E}'_{II}|^2, \tag{3.4}$$

where c is the speed of light in free space, $k' = \omega/c$, ϵ_0 is the permittivity of free space and ϵ' and $\epsilon'' = \sigma/\omega$ are the relative permittivity and loss factor respectively of the fluid. If the fluid is purely dipolar, then σ is the imaginary part of the dielectric constant. On the other hand, if the fluid is dipolar with conductive losses, then σ is the effective conductivity, Kriegsmann (1993). $\triangle = \frac{\partial^2}{\partial x'^2} + \frac{\partial^2}{\partial y'^2} + \frac{\partial^2}{\partial z'^2}$. The boundary conditions are those of no slip for fluid velocities at the solid walls

$$u_1' = u_2' = u_3' = 0, \qquad z = 0, d, \tag{3.5}$$

In the case of a free upper surface the boundary condition at $z = d$ becomes

$$\frac{\partial u_1'}{\partial y'} + \frac{\partial u_3'}{\partial x'} = \frac{\partial u_2'}{\partial x'} + \frac{\partial u_3'}{\partial y'} = 0, \quad u_3' = 0, \qquad z = d, \tag{3.6}$$

Convective conditions for the temperature are imposed at the walls

$$k_t \frac{\partial \theta'}{\partial z} = h(\theta' - \theta_o), \qquad z = 0, \tag{3.7}$$

$$k_t \frac{\partial \theta'}{\partial z} = -h(\theta' - \theta_o), \qquad z = d. \tag{3.8}$$

In equations (3.2-3.8) above g is the acceleration due to gravity, c_p is the specific heat of the fluid and h is the heat transfer coefficient measuring loss of heat due to

convective cooling. The source term in (3.4) is due to the microwave interaction with the fluid.

We impose the following continuity conditions on the tangential electric and magnetic fields at the slab boundaries; see Ramo et al. (1984), section 3.14.

$$(\nabla \times \mathbf{E}'_{II}) \times \hat{\mathbf{n}} = (\nabla \times \mathbf{E}'_{I}) \times \hat{\mathbf{n}}, \qquad z = 1, \tag{3.9}$$

$$(\nabla \times \mathbf{E}'_{II}) \times \hat{\mathbf{n}} = (\nabla \times \mathbf{E}'_{III}) \times \hat{\mathbf{n}}, \qquad z = 0, \tag{3.10}$$

$$\mathbf{E}'_{II} \times \hat{\mathbf{n}} = \mathbf{E}'_{I} \times \hat{\mathbf{n}}, \qquad z = 1, \tag{3.11}$$

$$\mathbf{E}'_{II} \times \hat{\mathbf{n}} = \mathbf{E}'_{III} \times \hat{\mathbf{n}}, \qquad z = 0, \tag{3.12}$$

where $\hat{\mathbf{n}}$ denotes the unit vector normal to the slab surfaces. The governing equations are made dimensionless by scaling distances with the slab thickness d, time by the diffusive time scale d^2/κ where $\kappa = k_t/(\rho_0 c_p)$ and the electric field by the incident amplitude E_0. New variables are introduced as

$$\begin{aligned} \mathbf{x} = \mathbf{x}'/d, \quad t = \kappa t'/(d^2), \quad \mathbf{u} = d\mathbf{u}'/\kappa \\ P = d^2/(\kappa^2 \rho_o) P', \quad \theta = (-1 + \frac{\theta'}{\theta_o}), \end{aligned} \tag{3.13}$$

New electric field variables are introduced as

$$E = E'/(e^{-ik'} E_0), \quad k = k'd, \tag{3.14}$$

Substitution of (3.13),(3.14) into (3.1-3.12) gives the dimensionless system given below. The nondimensional groups which enter into the dynamics are the Rayleigh number, R, the Prandtl number, Pr, the Biot number, β, and a nondimensional measure of the incident microwave power denoted by χ. These groups are given by:

$$R = (\alpha g d^3 \theta_o)/(\kappa\nu), \quad Pr = \nu/\kappa, \quad \beta = hd/k_t, \quad \chi = \epsilon''_0 \omega \epsilon_0 |E_o|^2 d^2/(2k_t\theta_o), \tag{3.15}$$

where ϵ''_0 is the dielectric loss factor of the fluid at reference temperature θ_0. These scalings give the following nondimensional system:

$$\triangle \mathbf{E}_{II} - \nabla(\nabla \cdot \mathbf{E}_{II}) + k^2 \left[\epsilon'(\theta) + i\epsilon''(\theta)\right] \mathbf{E}_{II} = 0, \tag{3.16}$$

$$\nabla \cdot \mathbf{u} = 0, \tag{3.17}$$

$$\frac{D\theta}{Dt} = \triangle\theta + \chi\epsilon''(\theta)|\mathbf{E}_{II}|^2, \tag{3.18}$$

$$\frac{D\mathbf{u}}{Dt} = -\nabla(p + \frac{d^3}{\kappa^2}gz) + RPr\theta\mathbf{k} + Pr\triangle\mathbf{u}, \tag{3.19}$$

$$(\nabla \times \mathbf{E}_{II}) \times \hat{\mathbf{n}} = (\nabla \times \mathbf{E}_I) \times \hat{\mathbf{n}}, \qquad z = 1, \tag{3.20}$$

$$(\nabla \times \mathbf{E}_{II}) \times \hat{\mathbf{n}} = (\nabla \times \mathbf{E}_{III}) \times \hat{\mathbf{n}}, \qquad z = 0, \tag{3.21}$$

$$\mathbf{E}_{II} \times \hat{\mathbf{n}} = \mathbf{E}_I \times \hat{\mathbf{n}}, \qquad z = 1, \tag{3.22}$$

$$\mathbf{E}_{II} \times \hat{\mathbf{n}} = \mathbf{E}_{III} \times \hat{\mathbf{n}}, \qquad z = 0, \tag{3.23}$$

$$\frac{\partial\theta}{\partial z} = \beta\theta, \qquad z = 0, \tag{3.24}$$

$$\frac{\partial\theta}{\partial z} = -\beta\theta, \qquad z = 1, \tag{3.25}$$

$$\underline{\text{No slip}} \qquad u_1 = u_2 = u_3 = 0, \qquad z = 0, 1, \tag{3.26}$$

3.2 Basic States

In the free space regions $z > 1$ and $z < 0$, the electric field is given by the real parts of

$$\mathbf{E} = E_0 \left[e^{-i(kz+\omega\tau)} + \gamma e^{i(kz-\omega\tau)}\right]\hat{\mathbf{j}}, \qquad z' > d, \tag{3.27}$$

$$\mathbf{E} = E_0 T e^{-i(kz+\omega\tau)}\hat{\mathbf{j}}, \qquad z' < 0, \tag{3.28}$$

respectively, where E_0 is the strength of the incident field, τ is the time scale of the electric field, T is the transmission coefficient, and γ is the reflection coefficient. Both T and γ are to be determined. The electric field which penetrates the fluid and interacts with it is given by the real part of $\mathbf{E} = [\psi(z)e^{-i\omega\tau}]\hat{\mathbf{j}}$, where ψ satisfies

$$\frac{d^2\psi}{dz^2} + k^2\left[\epsilon'(\bar{\theta}(z)) + i\epsilon''(\bar{\theta}(z))\right]\psi = 0, \qquad 0 < z < 1, \tag{3.29}$$

Note that the averaged microwave source term drives the heat equation. The electric field from the source is polarized in the y-direction and varies spatially in the z-direction only; Therefore, the steady-state temperature θ depends only on z and the governing equation 3.1 becomes:

$$\frac{d^2\bar{\theta}}{dz^2} = -\chi\epsilon''(\bar{\theta})|\psi|^2, \tag{3.30}$$

The boundary conditions on ψ are derived as in chapter 2 and given as:

$$\frac{d\psi}{dz} + ik\psi = 0, \qquad z = 0, \tag{3.31}$$

$$\frac{d\psi}{dz} - ik\psi = -2ik, \qquad z = 1, \tag{3.32}$$

Because the complex permittivity is temperature dependent, the differential equations governing the electric field and the temperature within the slab are now coupled. As a result, we must solve for the basic states numerically. The base velocity field is $\mathbf{u} = \mathbf{0}$. Utilizing the boundary conditions (3.24),(3.25) and (3.31),(3.32), we attain solutions for ψ and $\bar{\theta}$.

Figures 3.3a-d give plots of the basic temperature for different values of k with unit Biot number and $\chi = .56$. Solutions to the above system were obtained by employing the Newton-Raphson method in conjunction with the ode45 differential equations solver in Matlab. As can be seen, the position of the point of maximum temperature varies with k in the variable conductivity case. Data points for the dielectric properties of water, ϵ' and ϵ'' , at various temperatures were interpolated for computational purposes [14]. Figures 3.1 and 3.2 give plots of the relative dielectric permittivity and the relative dielectric loss factor, respectively, as functions of dimensionless temperature θ.

In the case of long microwaves, $k << 1$, it can be shown by the same arguments given in chapter 2 (section 2.2) that the electric field distribution in the fluid slab becomes unity. Consequently the temperature distribution is governed by the

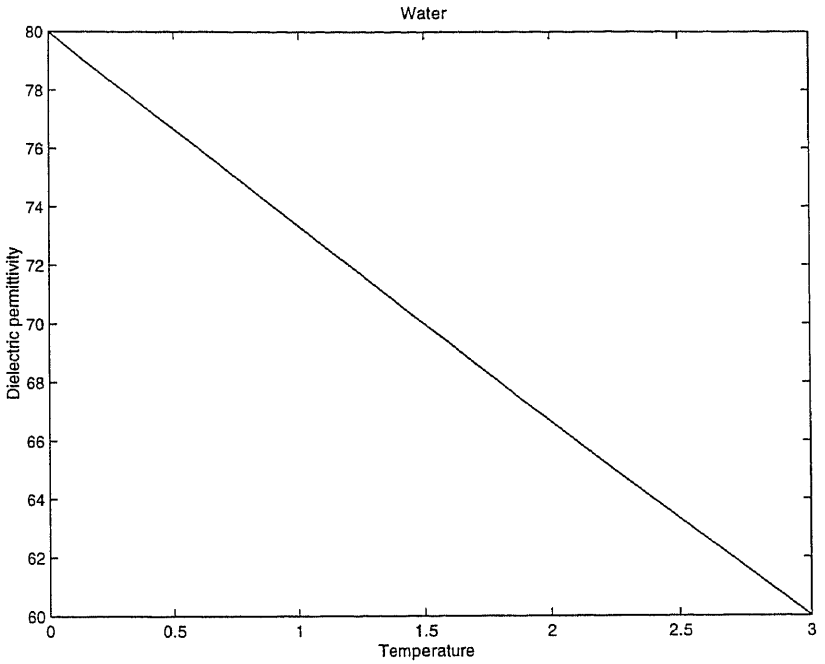

Figure 3.1 Dielectric permittivity of water vs. temperature;

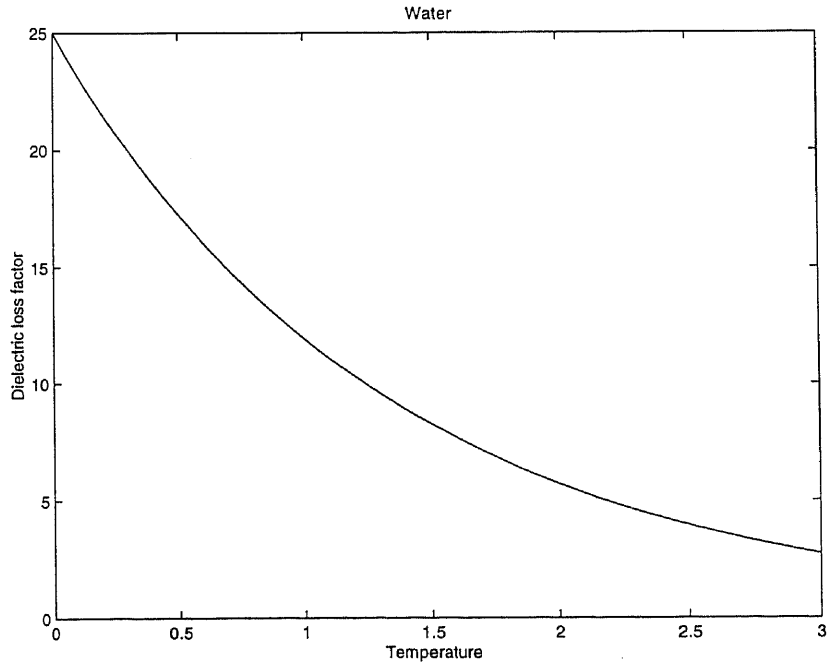

Figure 3.2 Dielectric loss factor of water vs. temperature;

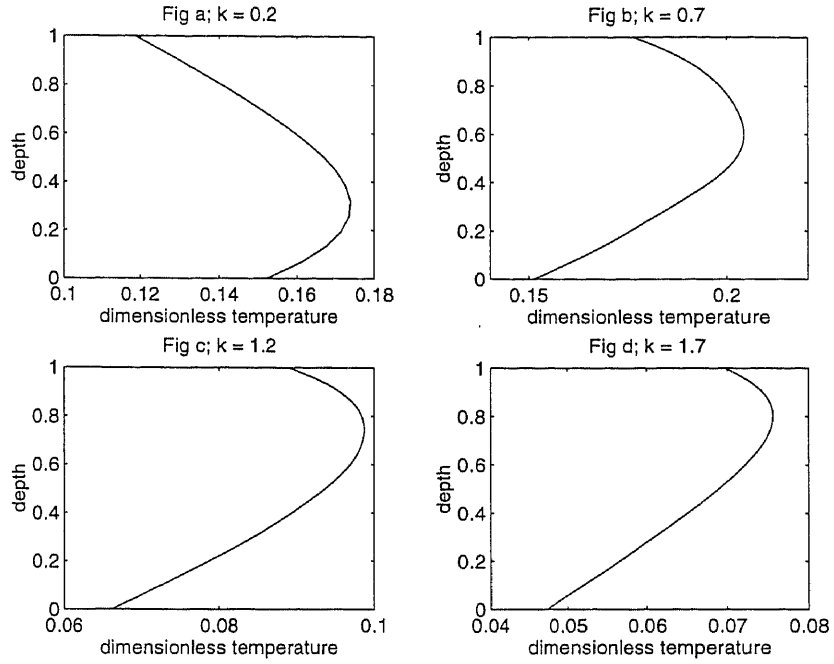

Figure 3.3 Undisturbed temperature profiles for water; $\beta = 1$.

following equation:

$$\frac{d^2\overline{\theta}}{dz^2} = -\chi\epsilon''(\overline{\theta}), \tag{3.33}$$

with the boundary conditions (3.24,3.25).

3.2.1 Thermal Runaway

A reasonable question to be asked in speaking about the stability of a fluid subjected to microwaves is the following: are the temperatures necessary to arouse instability within the fluid also temperatures at which thermal runaway can occur within a fluid. To arrive at a reasonable answer, one can investigate the worst case scenario in which the fluid is quiescent. Utilizing equations (3.29) and (3.30) along the boundary conditions (3.24),(3.25) and (3.31),(3.32) for $\bar{\theta}$ and ψ respectively, we can produce steady-state curves relating the incident power term χ to the maximum steady temperature θ_m within the fluid media. Figure 3.4 gives plots of θ_m versus χ for $k = 1, 2, 2.5$. The fluid considered in this study is water since much is known about its thermodynamic and dielectric properties. Observe that for the value $k = 2$,

there exists a power level χ beyond which the maximum temperature jumps from the lower branch of each steady-state curve to an upper branch of each curve. The new value of the maximum temperature reached for this curve lies below the boiling point. For $k = 2.5$, however, there is a threshold power beyond which the maximum temperature will jump up into the boiling regime. As will be seen in our investigation of the linear stability of the full system (3.16-3.26), these curves indicate that the power levels needed to achieve the onset of convection fall far below those at which any thermal runaway phenomena occurs. If the dielectric permittivity ϵ' and the dielectric loss factor ϵ'' are independent of θ then the curves shown in Figure 3.4 become monotonic. It is the decreasing behavior of ϵ' and ϵ'' with θ which causes the temperature distribution to profoundly effect the electric field within the slab. This is the root cause of the non-monotonic behavior of θ_m on k. Physically, altering k can be thought of as altering the thickness of the fluid slab. The neutral curves were computed using a secant-shooting method in conjuction with a Matlab ordinary differential equation solver.

An interesting case to investigate is the limiting case of nearly insulated boundaries or, equivalently, a small Biot number. Thermal runaway has been studied analytically in this limiting case in materials whose dielectric loss increases with temperature (Kriegsmann (1992)). Studies have also been conducted on fluids such as water where the dielectric loss and permittivity both decrease with temperature (Stuerga, More, Lallemant and Zahreddine (1993)). We reiterate some analysis here.

In the limit ($\beta << 1$), one can construct a leading order asymptotic approximation to the exact relation between χ and θ_m. We rewrite χ as $\chi_{run}\beta$ where β has its usual meaning and $\chi_{run} = \omega\epsilon_o''\epsilon_o|E_o|^2 d/(2hT_o)$. The system is given:

$$\frac{d^2\psi}{dz^2} + k^2\left[\epsilon'(\theta(z,t)) + i\epsilon''(\theta(z,t))\right]\psi = 0, \qquad 0 < z < 1, \tag{3.34}$$

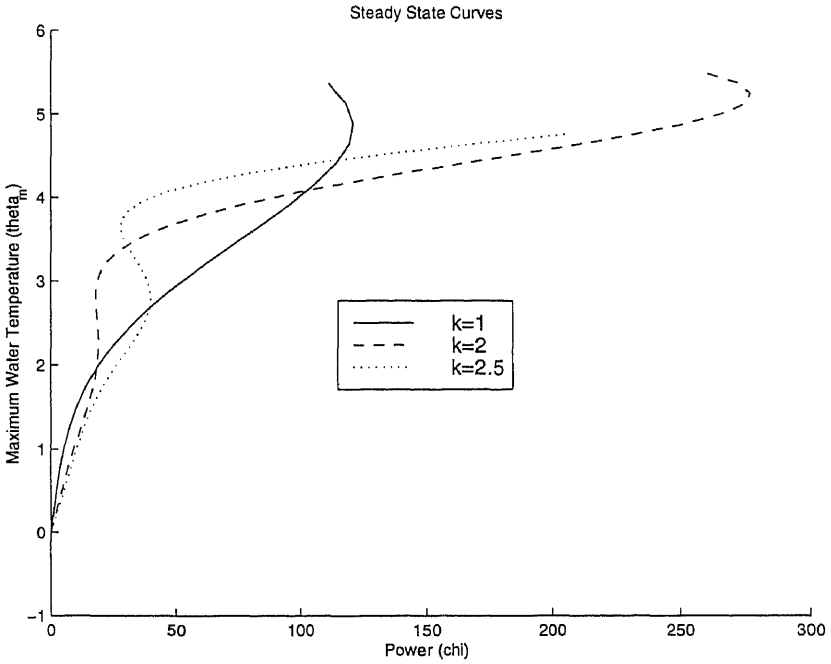

Figure 3.4 Steady-state curves for water (θ_m vs. χ); $\beta = 1$.

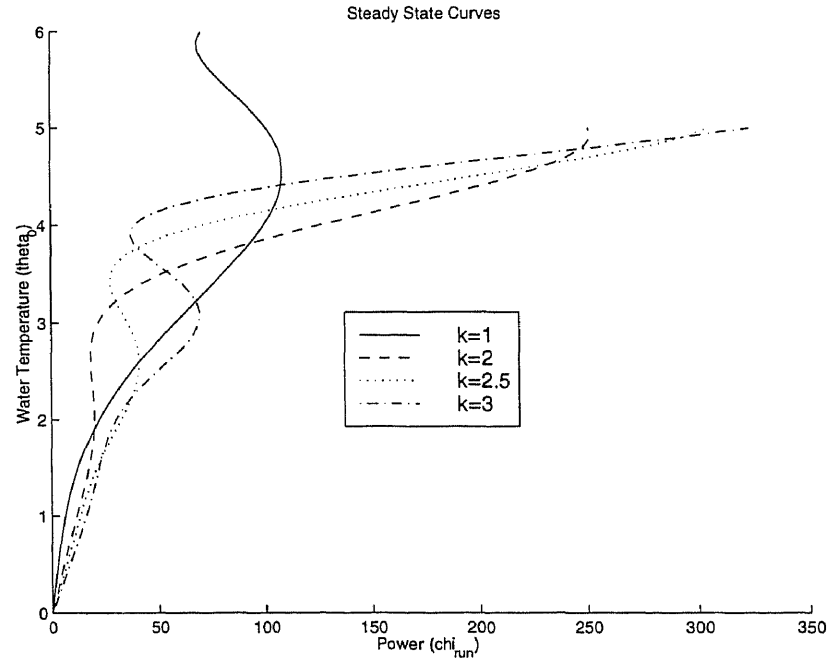

Figure 3.5 Steady-state curves for water (θ_0 vs. χ_{run}); $\beta << 1$

$$\frac{\partial \theta}{\partial t} = \frac{d^2\theta}{dz^2} + \chi_{run}\epsilon''(\theta)\beta|\psi|^2, \tag{3.35}$$

$$\frac{\partial \theta}{\partial z} = \beta, \theta \qquad z = 0, \tag{3.36}$$

$$\frac{\partial \theta}{\partial z} = -\beta, \theta \qquad z = 1, \tag{3.37}$$

$$\frac{d\psi}{dz} + ik\psi = 0, \qquad z = 0, \tag{3.38}$$

$$\frac{d\psi}{dz} - ik\psi = -2ik, \qquad z = 1, \tag{3.39}$$

Notice that the nondimensional heat source of (3.35) contains the Biot number and hence for $\chi \sim O(1)$ the source will be very small suggesting that the temperature will undergo a very slow evolutionary process in time t. This suggests the need the rescale time in favor of a slow time variable $\tau = \beta t$. In terms of τ, 3.35 becomes:

$$\beta\frac{\partial \theta}{\partial \tau} = \frac{d^2\theta}{dz^2} + \chi_{run}\epsilon''(\theta)\beta|\psi|^2, \tag{3.40}$$

Formally, θ and ψ are each expanded in a power series in β ($\theta = \theta_0(z,\tau) + \theta_1(z,\tau)\beta + \cdots$; $\psi = \psi_0 + \psi_1\beta + \cdots$). The coefficients in the powers of β are each set to zero yielding an infinite set of equations. We are interested in investigating the dynamic behavior of the temperature to leading order. Substituting the expansions above into (3.34),(3.40) and (3.36-3.39) we obtain the leading order system:

$$\frac{d^2\psi_0}{dz^2} + k^2\left[\epsilon'(\theta_0) + i\epsilon''(\theta_0)\right]\psi = 0, \qquad 0 < z < 1, \tag{3.41}$$

$$\frac{d^2\theta_0}{dz^2} = 0, \tag{3.42}$$

$$\frac{\partial \theta_0}{\partial z} = 0, \qquad z = 0, \tag{3.43}$$

$$\frac{\partial \theta_0}{\partial z} = 0, \qquad z = 1, \tag{3.44}$$

$$\frac{d\psi_0}{dz} + ik\psi_0 = 0, \qquad z = 0, \tag{3.45}$$

$$\frac{d\psi_0}{dz} - ik\psi_0 = -2ik, \qquad z = 1, \tag{3.46}$$

Notice that $\theta_0 = \theta_0(\tau)$. Since θ_0 does not depend on z, the leading order electric field can be solved exactly. In order to describe the steady-state temperature to leading order we must look at the energy equation and its boundary conditions to the next order $O(\beta)$:

$$\frac{\partial \theta_0}{\partial \tau} = \frac{d^2\theta_1}{dz^2} + \chi_{run}\epsilon''(\theta_o)|\psi_0|^2, \tag{3.47}$$

$$\frac{\partial \theta_1}{\partial z} = \theta_0, \qquad z = 0, \tag{3.48}$$

$$\frac{\partial \theta_1}{\partial z} = -\theta_0, \qquad z = 1, \tag{3.49}$$

Integrating (3.47) over the interval $0 < z < 1$, we arrive at ordinary differential equation for θ_0 or, equivalently, the leading order energy conservation equation:

$$\frac{d\theta_0}{d\tau} = -2\theta_0 + \chi_{run}\epsilon''(\theta_0)\int^1_0 |E_o|^2 dz, \tag{3.50}$$

Since E_0 is known, this equation along with an initial condition on θ_0 completely specifies $\theta_0(\tau)$. The steady-state equation is:

$$\frac{2\theta_0}{\epsilon''(\theta_0)\int^1_0 |E_o|^2 dz} = \chi_{run}, \tag{3.51}$$

Figure 3.5 gives steady-state curves for θ_o vs. the power term χ. The fluid studied is water. The curves are given for $k = 1, 2, 2.5, 3$. Recall that the parameter k can be thought of as the thickness of the slab. Physically we see that for $k = 1$, the temperature of the water changes continuously with the power term χ_{run} up to the boiling temperature. For $k = 2$ and $k = 2.5$ however, the steady-state curve has an "S" shape. This suggests the existence of a power level beyond which the leading order water temperature θ_o will jump from the lower branch of the neutral curve to the upper branch of the curve. The temperature on this new branch is still below the boiling point for these values of k. For $k = 3$, however, the upper branch of the steady curve lies just above the boiling point. So, for nearly insulated boundaries, the model suggests that thermal runaway is possible for water. This is possible because the dielectric attributes create a resonance of the electric field through their temperature dependence.

3.3 Linear Stability Theory

The linear stability of the undisturbed states described above can be analyzed by adding small perturbations $\mathbf{u}'$, θ', P' and $\mathbf{E}'$. Linearizing (3.16-3.26) with respect to primed quantities, we obtain:

$$-\triangle \mathbf{E}'_{II} + \nabla(\nabla \cdot \mathbf{E}'_{II}) = -k^2 \left(\epsilon_c(\bar{\theta}) \mathbf{E}'_{II} + \frac{d\epsilon_c(\bar{\theta})}{d\theta} \theta' \bar{\mathbf{E}} \right), \tag{3.52}$$

$$\frac{\partial \theta'}{\partial t} + \frac{\partial \bar{\theta}}{\partial z} w' = \triangle \theta' + \chi \left(\left(\psi \mathbf{E}'^{*}_{II} \hat{\mathbf{j}} + \psi^* \mathbf{E}'_{II} \hat{\mathbf{j}} \right) \epsilon''(\bar{\theta}) + \theta' \frac{d\epsilon''(\bar{\theta})}{d\theta} |\psi|^2 \right), \tag{3.53}$$

$$\frac{\partial \mathbf{u}'}{\partial t} = -\nabla p' - RPr\theta' \hat{\mathbf{k}} + Pr \triangle \mathbf{u}', \tag{3.54}$$

$$\nabla \cdot \mathbf{u}' = 0, \tag{3.55}$$

$$(\nabla \times \mathbf{E}'_{II}) \times \hat{\mathbf{n}} = (\nabla \times \mathbf{E}'_{I}) \times \hat{\mathbf{n}}, \qquad z = 1, \tag{3.56}$$

$$(\nabla \times \mathbf{E}'_{II}) \times \hat{\mathbf{n}} = (\nabla \times \mathbf{E}'_{III}) \hat{\mathbf{n}}, \qquad z = 0, \tag{3.57}$$

$$\mathbf{E}'_{II} \times \hat{\mathbf{n}} = \mathbf{E}'_{I} \times \hat{\mathbf{n}}, \qquad z = 1, \tag{3.58}$$

$$\mathbf{E}'_{II} \times \hat{\mathbf{n}} = \mathbf{E}'_{III} \times \hat{\mathbf{n}}, \qquad z = 0, \tag{3.59}$$

$$\frac{\partial \theta'}{\partial z} = \beta\theta', \qquad z = 0, \tag{3.60}$$

$$\frac{\partial \theta'}{\partial z} = -\beta\theta', \qquad z = 1, \tag{3.61}$$

$$\text{Rigid} - \text{rigid surface} \quad w' = \frac{\partial w'}{\partial z} = 0, \qquad z = 0, 1, \tag{3.62}$$

$$\text{Rigid} - \text{free surface} \quad \frac{\partial^2 w'}{\partial z^2} = 0, \qquad z = 1, \tag{3.63}$$

where the starred quantities denote complex conjugates and $\epsilon_c = \epsilon'(\bar{\theta}+\theta') + \epsilon''(\bar{\theta}+\theta')$ and $\bar{\theta}$ and ψ are the background temperature and electric field respectively. Taking the curl of (3.54) twice, we obtain the following equation involving the vertical velocity component of the fluid and the temperature:

$$\frac{\partial \triangle w'}{\partial t} = R\chi Pr \triangle_1 \theta' + Pr \triangle^2 w', \tag{3.64}$$

where $\triangle_1 = \frac{\partial^2}{\partial x^2} + \frac{\partial^2}{\partial y^2}$. This equation along with (3.53) and (3.52)will be used to determine the stability of the system. Note that with the eigenfunctions w' and θ' known the continuity equation (3.55) along with (3.54) yields the velocity components u' and v'.

The scalar equations for the electric field components within the slab are:

$$-\triangle E'_1 - J(z)\frac{\partial E'_3}{\partial x} - G(z)\frac{\partial^2 \theta'}{\partial x \partial y} = k^2 \epsilon_c(\bar{\theta}) E'_1, \tag{3.65}$$

$$-\triangle E'_2 - J(z)\frac{\partial E'_3}{\partial y} - G(z)\frac{\partial^2 \theta'}{\partial y^2} = k^2 \epsilon_c(\bar{\theta}) E'_2 + k^2 \frac{d}{d\theta}(\epsilon_c(\bar{\theta}))\theta'\psi, \tag{3.66}$$

$$-\triangle E'_3 - \frac{\partial}{\partial z}(JE'_3) - \frac{\partial}{\partial z}(G\frac{\partial \theta'}{\partial y}) = k^2 \epsilon_c(\bar{\theta}) E'_3, \tag{3.67}$$

where $J = \frac{d}{d\theta}(\epsilon_c(\bar{\theta}))\frac{d}{dz}(\bar{\theta})/\epsilon_c$; $G = \frac{d}{d\theta}(\epsilon_c(\bar{\theta}))\psi/\epsilon_c$

We now consider the case where $\mathbf{E} = \mathbf{E}(x, z, t)$ in which case $\mathbf{u} = \mathbf{u}(x, z, t)$ and $\theta = \theta(x, z, t)$. Note that we have dropped the primes from the perturbation terms.

Physically, we can think of convective rolls as corresponding to this two dimensional construction. From a qualitative standpoint, the two dimensional linear system is interesting in that it describes the manner in which the perturbation electric field actually feeds back into the heat equation and affects the stability of the system overall. Note that for a two dimensional disturbance E_2 is then decoupled from E_1 and E_3, and is the only component affecting the energy equation.

Given the following ansatz: $\theta = T(z)e^{iax+\sigma t} + c.c.$, $E_2 = \phi_1(z)e^{iax+\sigma t} + \phi_2(z)e^{-iax+\sigma^* t}$, $w = W(z)e^{iax+\sigma t} + c.c.$ describing two dimensional disturbances, we can analyze (3.52),(3.53) and (3.55-3.64) by separation of variables to arrive at a linearized ordinary differential system to be solved:

$$-(D^2 - a^2)\phi_1 - k^2\epsilon_c(\bar{\theta})\phi_1 = k^2\frac{d}{d\theta}\epsilon_c(\bar{\theta})T\psi, \tag{3.68}$$

$$-(D^2 - a^2)\phi_2{}^* - k^2\epsilon_c^*(\bar{\theta})\phi_2{}^* = k^2\frac{d}{d\theta}\epsilon_c^*(\bar{\theta})T\psi^*, \tag{3.69}$$

$$\sigma T + \frac{d\bar{\theta}}{dz}W = (D^2 - a^2)T + \chi(\psi^*\phi_1\epsilon''(\bar{\theta}) + \psi\phi_2{}^*\epsilon''(\bar{\theta})) + T\frac{d}{d\theta}(\epsilon''(\bar{\theta}))|\psi|^2, \tag{3.70}$$

$$\sigma(D^2 - a^2)W = -RPra^2T + (D^2 - a^2)^2W, \tag{3.71}$$

where $D = \frac{\partial}{\partial z}$. The boundary conditions on the electric field for $(k^2 \geq a^2)$ are:

$$\frac{d}{dz}\phi_1 - i\sqrt{(k^2 - a^2)}\phi_1 = 0, \qquad z = 1, \tag{3.72}$$

$$\frac{d}{dz}\phi_1 + i\sqrt{(k^2 - a^2)}\phi_1 = 0, \qquad z = 0, \tag{3.73}$$

For $(k^2 < a^2)$ they become:

$$\frac{d}{dz}\phi_1 + \sqrt{(a^2 - k^2)}\phi_1 = 0, \qquad z = 1, \tag{3.74}$$

$$\frac{d}{dz}\phi_1 - \sqrt{(a^2 - k^2)}\phi_1 = 0, \qquad z = 0, \tag{3.75}$$

$\phi_2{}^*$ satisfies the conjugate boundary conditions:

$$\frac{d}{dz}\phi_2{}^* + i\sqrt{(k^2 - a^2)}\phi_2{}^* = 0, \qquad z = 1, \tag{3.76}$$

$$\frac{d}{dz}\phi_2{}^* - i\sqrt{(k^2 - a^2)}\phi_2{}^* = 0, \qquad z = 0, \tag{3.77}$$

for $(k^2 \geq a^2)$ and

$$\frac{d}{dz}\phi_2{}^* + \sqrt{(a^2 - k^2)}\phi_2{}^* = 0, \qquad z = 1, \tag{3.78}$$

$$\frac{d}{dz}\phi_2{}^* - \sqrt{(a^2 - k^2)}\phi_2{}^* = 0, \qquad z = 0, \tag{3.79}$$

for $(k^2 < a^2)$.

The boundary conditions for θ and W are:

$$W = \frac{d}{dz}W = 0, \qquad z = 0, 1, \tag{3.80}$$

$$\theta = \beta\theta, \qquad z = 0, \tag{3.81}$$

$$\theta = -\beta\theta, \qquad z = 1, \tag{3.82}$$

3.4 Numerical Solutions

If the temperature dependence of the fluid's dielectric attributes is taken into account there is very little, analytically, that can be done to attain solutions to the mathematical problem. In order to solve for the basic states, we implemented a shooting method using a Newton-Raphson approach in conjunction with the Matlab ode45 ordinary differential equations solver routine. In the linear stability portion of the model this approach does work but the system is a tenth order differential system and the number of shooting variables is such that the run time is too long.

3.4.1 A Finite Difference Approach

The approach taken here to solve the linearized problem is to discretize the system (3.68-3.82) and pose the problem as a homogeneous system of algebraic equations. Having constructed the coefficient matrix, we then implement Newton's method to find the eigenvalue of the problem. For example, the curves of Figure 3.6 are generated by searching for the roots of the determinant of the coefficient matrix which is parameterized by the eigenvalue σ, all other parameters being fixed. The curves

in Figure 3.7 are generated by shooting on the parameter χ, with σ set identically to zero. Note that the Newton iteration procedure is more involved here since χ enters explicitly into the basic state energy equation as well as the coefficient matrix of the linearized system.

The following is the discretization for the system (3.68-3.82) on the interval [0,1] where the discretization step size is $\triangle z$, $z_j = (j-1)\triangle z$ and $(j = 1, \ldots, N+1)$. In approximating the derivatives, central difference methods are employed giving $O(\triangle z^2)$ accuracy on the interior points.

$$\phi_{1j-1} + \phi_{1j}A_j + \phi_{1j+1} + T_jB_j = 0, \tag{3.83}$$

$$\phi^*_{2j-1} + \phi^*_{2j}A^*_j + \phi^*_{2j+1} + T_jB^*_j = 0, \tag{3.84}$$

$$T_{j-1} + T_jC_j + T_{j+1} + \phi_{1j}D_j + \phi^*_{2j}E_j + w_j\frac{d\bar{\theta}}{dz} = 0, \tag{3.85}$$

$$w_{j-2} + w_{j-1}F + w_jG + w_{j+1}F + w_{j+2} - T_jh^4a^2R = 0, \tag{3.86}$$

where

$$A_j = \left(-2 + \triangle z^2(k^2\epsilon_c(\bar{\theta}) - a^2)\right), \quad B_j = \triangle z^2k^2\tfrac{d}{d\theta}\epsilon_c(\bar{\theta})\psi$$
$$C_j = \left(-2 + \triangle z^2(-\sigma - a^2 + \tfrac{d}{d\theta}\epsilon''(\bar{\theta})|\psi|^2\chi)\right), \quad D_j = \psi^*\chi\epsilon''(\bar{\theta}), \quad E_j = \psi\chi\epsilon''(\bar{\theta})$$
$$F = \left(-4 - \triangle z^2(2a^2 + \sigma/Pr)\right), \quad G = \left(6 + \triangle z^2(4a^2 + 2\sigma/Pr) + \triangle z^4(a^4 + a^2\sigma/Pr)\right)$$

The boundary conditions of the system are of mixed type and straight forward one-sided difference methods give $O(\triangle z)$ accuracy. We employ fictitious points $z_o = -\triangle z$ and $z_{N+2} = 1 + \triangle z$ to preserve $O(\triangle z^2)$ accuracy, as explained below. The corresponding boundary conditions are for ($j = 1$ corresponding to the boundary $z = 0$):

$$\phi_{10} = 2\triangle zi\sqrt{k^2 - a^2}\phi_{11} + \phi_{12}, \qquad k^2 >= a^2, \tag{3.87}$$

$$\phi^*_{20} = -2\triangle zi\sqrt{k^2 - a^2}\phi^*_{21} + \phi^*_{22}, \qquad k^2 >= a^2, \tag{3.88}$$

$$\phi_{10} = -2\triangle z\sqrt{a^2 - k^2}\phi_{11} + \phi_{12}, \qquad k^2 < a^2, \tag{3.89}$$

$$\phi^*_{20} = -2\triangle z\sqrt{a^2 - k^2}\phi^*_{21} + \phi^*_{22}, \qquad k^2 < a^2, \tag{3.90}$$

$$w_0 = w_2, \quad w_1 = 0, \tag{3.91}$$

$$T_0 = T_2 - 2h\beta T_1, \tag{3.92}$$

for ($j = N + 1$ corresponding to the boundary $z = 1$):

$$\phi_{1N+2} = 2\triangle zi\sqrt{k^2 - a^2}\phi_{1N+1} + \phi_{1N}, \qquad k^2 >= a^2, \tag{3.93}$$

$$\phi^*_{2N+2} = -2\triangle zi\sqrt{k^2 - a^2}\phi^*_{2N+1} + \phi^*_{2N}, \qquad k^2 >= a^2, \tag{3.94}$$

$$\phi_{1N+2} = -2\triangle z\sqrt{a^2 - k^2}\phi_{1N+1} + \phi_{1N}, \qquad k^2 < a^2, \tag{3.95}$$

$$\phi^*_{2N+2} = -2\triangle z\sqrt{a^2 - k^2}\phi^*_{2N+2} + \phi^*_{2N}, \qquad k^2 < a^2, \tag{3.96}$$

$$w_{N+2} = w_N, \quad w_{N+1} = 0, \tag{3.97}$$

$$T_{N+2} = T_N - 2h\beta T_{N+1}, \tag{3.98}$$

The unknowns ϕ_{10}, ϕ^*_{20}, w_0, T_0 and ϕ_{1N+2}, ϕ^*_{2N+2}, w_{N+2}, T_{N+2} can all be eliminated from (3.87-3.98) by employing central differences of the equations (3.83-3.86) at $z = 0$ and $z = 1$ respectively. The modified equations are as follows:

for $j = 1$ the system is given as:

$$\phi_{11}A'_1 + 2\phi_{12} + T_1B_1 = 0, \tag{3.99}$$

$$\phi^*_{21}A'^*_1 + 2\phi^*_{22} + T_1B^*_1 = 0, \tag{3.100}$$

$$T_1C'_1 + 2T_2 + \phi_{11}D_1 + \phi^*_{21}E_1 = 0, \tag{3.101}$$

Since $w_1 = 0$, the momentum equation does not enter here. For $j = 2$ the only equation modified in the system (3.83-3.86) is (3.86) which becomes:

$$w_2(G + 1) + w_3F + w_4 - T_2\triangle z^4a^2R = 0, \tag{3.102}$$

for $j = N$ equation (3.86) becomes:

$$w_{N-2} + w_{N-1}F + w_N(G + 1) - T_N\triangle z^4a^2R = 0, \tag{3.103}$$

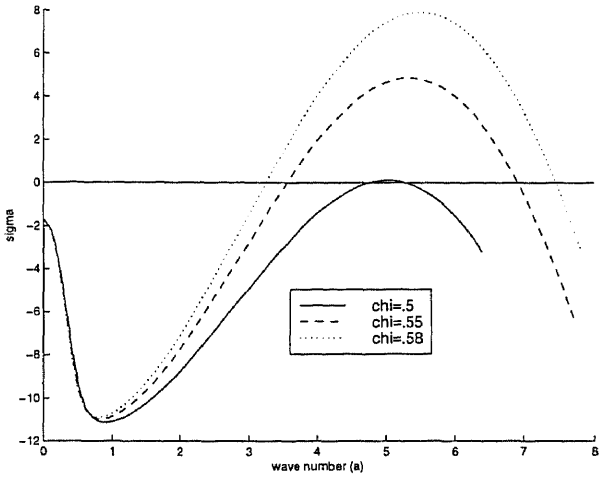

Figure 3.6 Growth rate curves, rigid-rigid case; $\beta = 1$; $k = 1$; $Pr = 7$.

for $j = N + 1$ the system becomes:

$$2\phi_{1N} + \phi_{1N+1}A'_{N+1} + T_{N+1}B_{N+1} = 0, \tag{3.104}$$

$$2\phi^*_{2N} + \phi^*_{2N+1}A'^*_{N+1} + T_{N+1}B^*_{N+1} = 0, \tag{3.105}$$

$$2T_N + T_{N+1}C'_{N+1} + \phi_{1N+1}D_{N+1} + \phi^*_{2N+1}E_{N+1} = 0, \tag{3.106}$$

where $A'_j = A_j + 2i\triangle z\sqrt{k^2 - a^2}$ if $k^2 \geq a^2$, $A'_j = A_j - 2\triangle z\sqrt{a^2 - k^2}$ if $k^2 < a^2$, $C'_j = C_j - 2\triangle z\beta$. The discretized system is now $O(\triangle z^2)$ accurate.

3.5 Results

The stability characteristics were obtained by fixing the physical parameters including the microwave power which is represented as the nondimensional variable χ. For different wavenumbers a, the eigenvalue σ, which is complex in general, was computed by iteration. Our numerical results produce real values of σ alone, indicating that there is no propagation of disturbances down the slab. This would be expected even with the introduction of temperature dependent dielectric attributes since there is no physical mechanism present to motive propagation of a disturbance in a preferred horizontal direction. As a result, neutral curves can be traced by

specifying $\sigma = 0$. A typical set of results is given in Figure 3.6 for different power settings (values of χ) and physical parameters corresponding to water. Water was chosen to be the subject fluid as there exist data for the dielecric permittivity and loss factors (ϵ' and ϵ'') for $0 \leq \bar{\theta} < 4$ for a microwave frequency of around 2.45 GHZ. As can be seen, larger values of χ support a larger band of unstable modes which narrows as the value of χ decreases-see the curves corresponding to $\chi = .58$ and $\chi = .55$. As the microwave power is decreased further, it reaches a value below which no mode becomes excited (slightly below $\chi = .5$).

Next we use typical stability plots, as in Figure 3.6, to present neutral curves which have $\sigma = 0$. For a fixed χ it is seen that there are at most two values of the wavenumber where the flow is neutrally stable, and below a critical value of χ, denoted by χ_c, the flow becomes linearly stable to all wave numbers. Neutral curves of χ against a for different Biot numbers (other parameters being fixed) are considered first. In Figure 3.7 we show neutral curves for $\beta = 0.1$ and 1.0 when the non-dimensional parameter $k = 1.0$. The unstable and stable regions are located above and below the given neutral curve respectively. In fact each neutral curve provides a critical minimum point (a_c, χ_c); flows corresponding to Rayleigh numbers below χ_c are stable. The variation of (a_c, χ_c) in parameter studies provides a lot of information about the stability characteristics and is considered later. Physically, β may be associated with the rate at which heat is convected away from the slab and hence an increase in the Biot number has a stabilizing effect on the system. That is, for a given value of χ the window of unstable modes contributing to the disturbance in the fluid decreases.

Figure 3.8 gives the variation of the critical values of χ_c with k, the ratio of slab thickness to microwave length. Figure 3.9 is a plot of the critical wavenumber a_c versus k, and Figure 3.10 presents the variation of the height where the background temperature achieves its maximum with k. The critical values for χ are those values

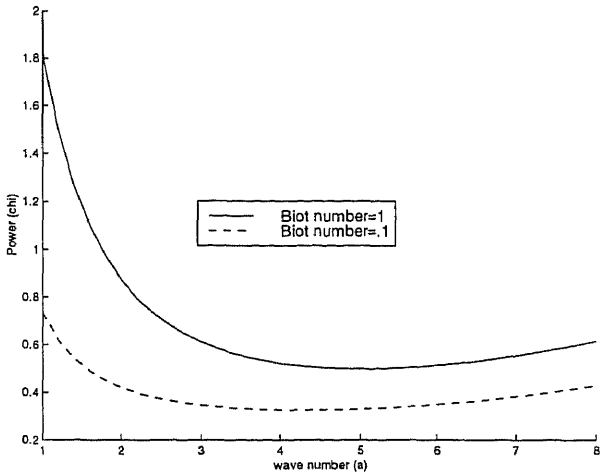

Figure 3.7 Neutral stability curves in the χ-a plane for water; $k = 1$.

at which the onset of instability is achieved and exactly one perturbation mode corresponding to the critical wave number a_c becomes excited. We note that the plots in Figure 3.8 have an oscillatory like behavior as k varies. The plots where constructed based on physical parameters for pure water. We compare the plots obtained when water is assumed to have a constant dielectric conductivity with those obtained when temperature dependence is taken into account. Note that in the case of constant permittivity the values used are at the reference temperature $\theta_0 = 0$. (see Figures 3.2 and 3.1). Observe that for certain values of k ($.2 \leq k \leq .27$ and $.43 \leq k \leq .5$) the assumption of a constant complex dielectric permittivity leads to lower estimates on of the power term χ at which the onset of instability occurs than does the assumption of a temperature dependent complex permittivity. For all other values of k, the opposite is true. The two curves are out of phase for smaller values of k, but become more syncronized as k gets larger. This may be explained by the fact that the largest fluctuations in the maximum temperature T_m at onset are seen for smaller values of k (see Figure 3.11) and hence, the dielectric permittivity $\epsilon'(\bar{\theta})$ and the dielectric loss factor $\epsilon''(\bar{\theta})$ vary significantly from their values at the reference temperature. As k increases, however, these fluctuations decrease as does the overall maximum temperature of the fluid as seen in the figure. As was mentioned in section

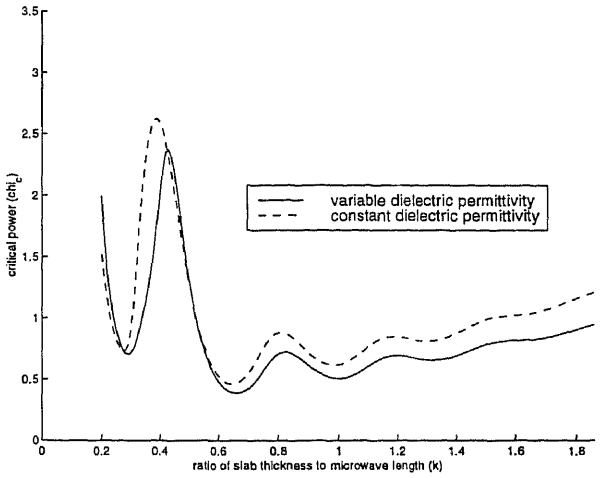

Figure 3.8 Neutral curves in the $\chi_c - k$ plane for water, rigid-rigid case: $\beta = 1$; $k = 1$.

3.2.1, there is a strong coupling between the temperature $\bar{\theta}$ and the electric field ψ through the fluids dielectric properties $\epsilon'(\bar{\theta})$ and $\epsilon''(\bar{\theta})$. These dielectric properties have a significant effect on the resonance of ψ within the fluid layer and hence, on the shape of the basic temperature profile. For example, for $.3 < k < .4$, it is seen in Figure 3.10 that when the temperature dependence of the dielectric properties of water is taken into account, the height of maximum temperature within the fluid layer is less than if this temperature dependence is neglected. If the height of the maximum temperature is lower, then a larger unstable fluid layer resides at the upper boundary. As a result, less power is necessary to achieve an onset of instability (see Figure 3.8) and such an instability can be achieved at lower temperatures. The fact that the curves of Figures 3.8-3.11 are in phase for both the case of constant complex permittivity and temperature dependent complex permittivity, is justified by arguments similar the those given for the constant conductivity case (see chapter2).

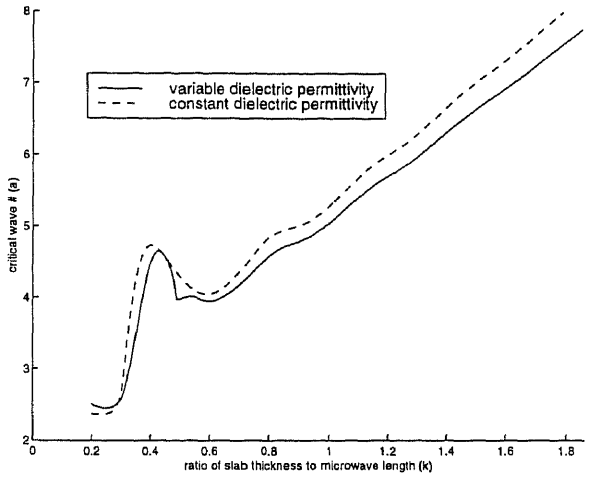

Figure 3.9 Neutral curves for water (critical wave number vs. k), rigid-rigid case: $\beta = 1$; $k = 1$.

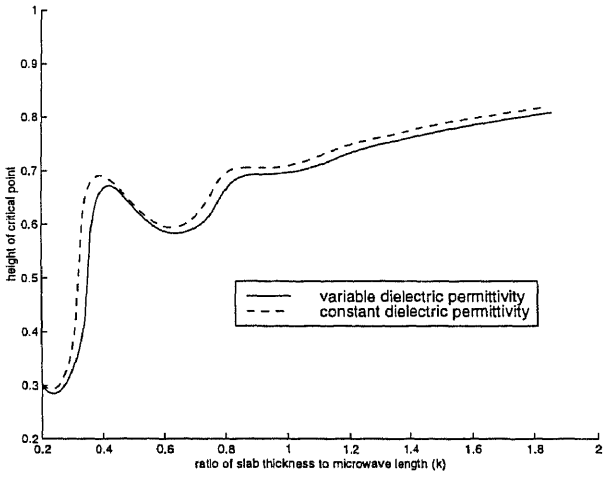

Figure 3.10 Neutral curves for water (height of maximum temperature vs. k), rigid-rigid case: $\beta = 1$; $k = 1$.

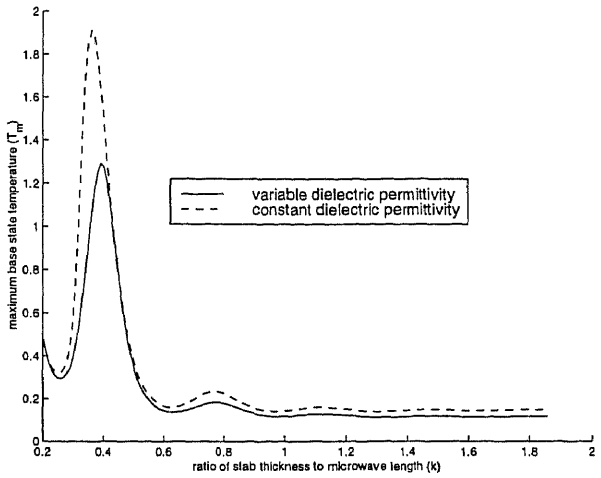

Figure 3.11 Neutral curves for water (maximum temperature vs. k), rigid-rigid case: $\beta = 1$; $k = 1$.

3.6 Discussion

The model considered in this chapter takes into account more of the physics involved in the interaction of a fluid with microwaves in that it incorporates the temperature dependence of the dielectric attributes of the fluid. Such a model is of importance in order to achieve greater accuracy on the power requirements to achieve the onset of instability where temperature variations within the slab are significant. As was seen for water, there are intervals of k where the monotonic decreasing behavior of the dielectric loss factor $\epsilon''(\bar{\theta})$ and the dielectric permittivity $\epsilon'(\bar{\theta})$ with temperature reduces the critical power level χ_c necessary to achieve an onset of instability. So, in these regimes, ignoring the temperature dependence of the dielectric properties of water on temperature would lead one to over estimate the incident critical microwave power necessary to achieve onset. There are, yet, other intervals where assumption of constant dielectric properties would lead us to underestimate this critical power. In carrying out industrial applications where one often wishes to use the least amount of power possible, the results discussed have important implications.

Figures 3.4 and 3.8 indicate that the power levels needed to achieve an onset of convection fall far below those necessary to experience thermal runaway phenomena

in water. What is interesting about Figures 3.4 and 3.5 is that they illustrate the importance of geometry in achieving thermal runaway. It was seen that by varying the thickness k of the fluid layer, one can alter both the temperature and microwave power level at which thermal runaway takes place. This may have important implications in commercial processes such as microwave processing of foods or other water-based materials.

CHAPTER 4

A MODEL FOR MELTING OF SOLIDS USING MICROWAVES

4.1 A Physical Overview (The Stefan Condition)

The physical system presented here consists of a two dimensional material of infinite extent in the x direction which is heated by a microwave source. Specifically we assume the existence of a time harmonic plane wave which impinges normally to the top face of the material. This electric field is taken to be polarized in the x direction. The material consists of two phases, liquid and solid, of a substance. The interface bounding the two phases is referred to as the melting front. One main objective is to track the position of the melting front in time. As can be seen in figure 4.1, there exist energy equations for both the solid and liquid phases which govern the temperature distribution in each of the respective regions. We let ϕ_1 and ϕ_2 represent the electric field distributions in the liquid and solid phases respectively, and $T_1(z)$ and $T_2(z)$ are the corresponding temperature distributions in the respective regions and κ_1 and κ_2 the corresponding thermal conductivities. Figure 4.2 illustrates the physics governing the movement of the melting front $S(t)$. At the melting front there exists an energy flux into the front from the liquid side $-\kappa_1 \frac{dT_1}{dz}$, and an energy flux out of the front on the solid side $\kappa_2 \frac{dT_2}{dz}$. If these fluxes are not in balance then the excess energy is consumed in facilitating a phase change of the solid into liquid at a rate $\rho\alpha \frac{dS}{dt}$. Hence the difference in these fluxes at time t determines the velocity of the melting front $\frac{dS}{dt}$.

This is the Stefan condition:

$$-\kappa_1 \frac{dT_1}{dz} + \kappa_2 \frac{dT_2}{dz} = \rho\alpha \frac{dS}{dt}, \tag{4.1}$$

α is the latent heat of melting and ρ is the density of the solid. Note that the front maintains a constant temperature known as the freezing temperature which is denoted as T_f.

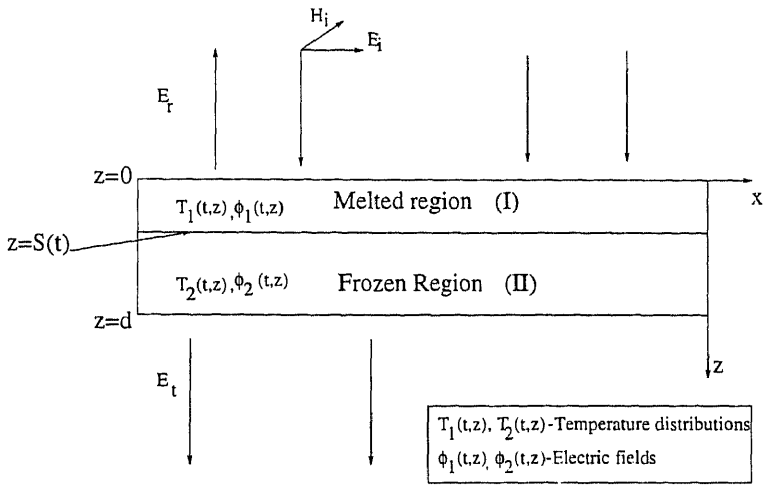

Figure 4.1 The geometry of the melting problem.

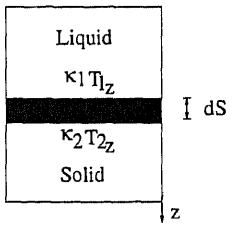

$\rho\alpha\, dS$-energy consumed to melt solid

$\kappa_1 T_{1z}$ -energy flux into region

$\kappa_2 T_{2z}$-energy flux out of region

$-\kappa_1 T_{1z} + \kappa_2 T_{2z} = \rho\alpha S_t$ ← The latent heat balance (Stefan) condition

ρ – density of solid α– latent heat of melting

Figure 4.2 The physics governing the moving front.

4.2 The Mathematical Model

We present the dimensional model governing the electric fields and temperature profiles within the liquid and solid phases of the material.

$$\frac{d^2\phi_1'}{dz^2} + k^2(\alpha_1\epsilon_1'(T_1') + \sigma_1\epsilon_1''(T_1'))\phi_1' = 0, \quad 0 < z < S'(t), \tag{4.2}$$

$$\frac{d^2\phi_2'}{dz^2} + k^2(\alpha_2\epsilon_2'(T_2') + \sigma_2\epsilon_2''(T_2'))\phi_2' = 0, \quad S'(t) < z < 1, \tag{4.3}$$

$$\frac{\rho_1 c_1}{\kappa_1}\frac{\partial T_1'}{\partial t'} = \frac{\partial^2 T_1'}{\partial z'^2} + \frac{\omega\epsilon_o\sigma_1\epsilon_1''}{2\kappa_1}|\phi_1'|^2, \quad 0 < z < S'(t), \tag{4.4}$$

$$\frac{\rho_2 c_2}{\kappa_2}\frac{\partial T_2'}{\partial t'} = \frac{\partial^2 T_2'}{\partial z'^2} + \frac{\omega\epsilon_o\sigma_2\epsilon_2''}{2\kappa_2}|\phi_2'|^2, \quad S'(t) < z < 1, \tag{4.5}$$

where ϵ_1' and ϵ_1'' are the relative dielectric permittivity and loss factor, respectively, of the liquid region and ϵ_2' and ϵ_2'' are the relative dielectric permittivity and loss factor, respectively, of the solid region: Also, α_1 and α_2 are values of the dielectric permittivities of these respective regions at the reference temperature which we denote as T_o, and σ_1 and σ_2 are the values of the loss factors at this temperature; $k = \omega/c$ where ω is the frequency of the impinging electromagnetic wave and c is the speed of light in free space; c_1 and c_2 are the specific heats of the liquid and solid regions respectively and ϵ_o is the dielectric permittivity of free space. Note that (4.4),(4.5) are driven by time averaged electric field sources. The time averaging is justified by the fact that the plane wave oscillates on a time scale which is much smaller than the thermal diffusive time scale of both the solid and liquid phases of the dielectric (see Appendix A). Manipulating Maxwell's equations, we arrive at ordinary differential equations governing the electric fields in the solid and liquid regions.

The electric field in the free space above the material has the form:

$$\phi_0 = E_0(e^{ikz} + \gamma e^{-ikz}) \tag{4.6}$$

The transmitted electric field in the free space region below the material has the form:

$$\phi_0 = E_0 T e^{ikz}, \tag{4.7}$$

where E_0 is the amplitude of the incident wave, γ is the reflection coefficient and T is the transmission coefficient. At dielectric interfaces, we impose conditions of continuity of both the tangential electric and magnetic fields (see Van Duzer, Ramo, section 3.14). Continuity of the tangential magnetic field is equivalent to continuity of the normal derivative of the electric field at $z = 0$ and $z = d$. These conditions yield the following equations:

$$\phi_1' = E_0(e^{ikz} + \gamma e^{-ikz}) \qquad z = 0, \tag{4.8}$$

$$\frac{d\phi_1'}{dz} = ikE_0(e^{ikz} - \gamma e^{-ikz}) \qquad z = 0, \tag{4.9}$$

Eliminating γ in favor of ϕ_1', the boundary condition 4.9 becomes:

$$\frac{d\phi_1'}{dz} + ik\phi_1' = 2ikE_o, \qquad z = 0, \tag{4.10}$$

Applying these similar conditions at the bottom face gives:

$$\frac{d\phi_2'}{dz} - ik\phi_2' = 0, \qquad z = d, \tag{4.11}$$

On the interface $S'(t)$ separating the liquid and solid phases, the boundary conditions are those of continuity of electric and magnetic fields, ie

$$\phi_1' = \phi_2', \quad \frac{d\phi_1'}{dz} = \frac{d\phi_2'}{dz}, \qquad z = S'(t), \tag{4.12}$$

The boundary conditions on the temperatures T_1' and T_2' in the liquid and solid portions, respectively, of the material are given by:

$$\kappa_1 \frac{\partial T_1'}{\partial z} = -h(T_1' - T_o), \qquad z = 0, \tag{4.13}$$

$$T_1' = T_2' = 0, \qquad z = S'(t), \tag{4.14}$$

$$T_2' = T_{bw}, \qquad z = d, \tag{4.15}$$

$$-\kappa_1 \frac{dT_1'}{dz} + \kappa_2 \frac{dT_2'}{dz} = \rho\alpha \frac{dS'}{dt}, \qquad z = S'(t), \tag{4.16}$$

where h is the heat transfer coefficient at the upper surface and T_{bw} is some fixed temperature.

The following scalings are introduced:

$$z = z'/d \qquad t = t'\kappa_2/(d^2\rho_2 c_2) \qquad T_1 = (T_1' - T_f)/(T_o - T_f)$$

$$\phi_1 = \phi_1'/(E_0) \qquad \phi_2 = \phi_2'/(E_0) \qquad T_2 = (T_2' - T_f)/(T_o - T_f)$$

$$\delta = \sigma_2/\sigma_1 \qquad \lambda = \kappa_2/\kappa_1 \qquad \mu = \rho_1 c_1/(\rho_2 c_2)$$

$$\beta = hd/\kappa_1 \qquad L = (\alpha\lambda)/((T_o - T_f)c_2)$$

$$\xi = \alpha_2/\alpha_1 \qquad P = \sigma_1\omega\epsilon_o d^2|E_o|^2/(2(T_o - T_f)\kappa_1)$$

With these scalings, we have the following dimensionless system:

$$\frac{d^2\phi_1}{dz^2} + k^2(\alpha_1\epsilon_1'(T_1) + i\sigma_1\epsilon_1''(T_1))\phi_1 = 0, \quad 0 < z < S(t), \tag{4.17}$$

$$\frac{d^2\phi_2}{dz^2} + k^2(\alpha_1\xi\epsilon_2'(T_2) + i\sigma_1\delta\epsilon_2''(T_2))\phi_2 = 0, \quad S(t) < z < 1, \tag{4.18}$$

$$\mu\lambda\frac{\partial T_1}{\partial t} = \frac{\partial^2 T_1}{\partial z^2} + P\epsilon_1''(T_1)|\phi_1|^2, \quad 0 < z < S(t), \tag{4.19}$$

$$\frac{\partial T_2}{\partial t} = \frac{\partial^2 T_2}{\partial z^2} + P\frac{\delta}{\lambda}\epsilon_2''(T_2)|\phi_2|^2, \quad S(t) < z < 1, \tag{4.20}$$

$$\frac{\partial T_1}{\partial z} = \beta(T_1 - 1), \qquad z = 0, \tag{4.21}$$

$$T_1 = T_2 = 0, \qquad z = S(t), \tag{4.22}$$

$$T_2 = T_{bw}, \qquad z = 1, \tag{4.23}$$

$$\frac{d\phi_1}{dz} + ik\phi_1 = 2ik, \qquad z = 0, \tag{4.24}$$

$$\phi_1 = \phi_2, \qquad z = S(t), \tag{4.25}$$

$$\frac{d\phi_1}{dz} = \frac{d\phi_2}{dz}, \qquad z = S(t), \tag{4.26}$$

$$\frac{d\phi_2}{dz} - ik\phi_2 = 0, \qquad z = 1, \tag{4.27}$$

The nondimensional Stefan condition is:

$$-\frac{dT_1}{dz} + \lambda\frac{dT_2}{dz} = L\frac{dS}{dt}, \qquad z = S(t), \tag{4.28}$$

At time $t = 0$, we let $T_1 = f(z)$ and $T_2 = g(z)$. This system comprises the full initial value problem to be solved.

4.3 The Case of Constant Dielectric Permittivity

4.3.1 Steady-State Solutions

It is of importance in melting applications, to know how much of a material will melt for a given power level of a microwave source. If there exists only one melting front within a material, it is enough to determine the steady-state position of the melting front S_{eq} for a given power level P. To find the steady-state solutions of the system (4.17-4.28), we set the time derivatives of this system to zero. The equations are given as:

$$\frac{d^2\phi_{1eq}}{dz^2} + k^2(\alpha_1\epsilon_1' + i\sigma_1\epsilon_1'')\phi_{1eq} = 0, \quad 0 < z < S_{eq}, \tag{4.29}$$

$$\frac{d^2\phi_{2eq}}{dz^2} + k^2(\alpha_1\xi\epsilon_2' + i\sigma_1\delta\epsilon_2'')\phi_{2eq} = 0, \quad S_{eq} < z < 1, \tag{4.30}$$

$$\frac{\partial^2 T_{1eq}}{\partial z^2} = -P\epsilon_1''|\phi_{1eq}|^2, \quad 0 < z < S_{eq}, \tag{4.31}$$

$$\frac{\partial^2 T_{1eq}}{\partial z^2} = -P\frac{\delta}{\lambda}\epsilon_2''|\phi_{2eq}|^2 \quad S_{eq} < z < 1, \tag{4.32}$$

$$\frac{\partial T_{1eq}}{\partial z} = \beta(T_{1eq} - 1), \qquad z = 0, \tag{4.33}$$

$$T_{1eq} = T_{2eq} = 0, \qquad z = S_{eq}, \tag{4.34}$$

$$T_{2eq} = T_{bw}, \qquad z = 1, \tag{4.35}$$

$$\frac{d\phi_{1eq}}{dz} + ik\phi_{1eq} = 2ik, \qquad z = 0, \tag{4.36}$$

$$\phi_{1eq} = \phi_{2eq} \qquad z = S_{eq}, \tag{4.37}$$

$$\frac{d\phi_{1eq}}{dz} = \frac{d\phi_{2eq}}{dz}, \qquad z = S_{eq}, \tag{4.38}$$

$$\frac{d\phi_{2eq}}{dz} - ik\phi_{2eq} = 0, \qquad z = 1, \tag{4.39}$$

The nondimensional Stefan condition is:

$$-\frac{dT_{1eq}}{dz}+\lambda\frac{dT_{2eq}}{dz}=0, \qquad z=S_{eq}, \tag{4.40}$$

With the assumption of constant dielectric attributes, ϵ_1', ϵ_2', ϵ_1'',and ϵ_2'' are unity. Observe that equations (4.29) and (4.30) are decoupled from the heat equations in the solid and liquid regions. Using these, together with the boundary conditions (4.36)-(4.39), we can deduce an exact solution for the electric fields in both the liquid and solid portions of the material. The solutions are given as:

$$\phi_{1eq}=c_1e^{-i\Gamma_1 z}+c_2e^{i\Gamma_1 z}, \tag{4.41}$$

$$\phi_{2eq}=c_3e^{-i\Gamma_1 z}+c_4e^{i\Gamma_1 z}, \tag{4.42}$$

where c_1 through c_4 satisfy the following linear algebraic system which is derived from equations (4.37-4.39):

$$\begin{pmatrix} \Gamma_1+k & -\Gamma_1+k & 0 & 0 \\ e^{i\Gamma_1 S_{eq}} & e^{-i\Gamma_1 S_{eq}} & -e^{i\Gamma_2 S_{eq}} & -e^{-i\Gamma_2 S_{eq}} \\ \Gamma_1 e^{i\Gamma_1 S_{eq}} & -\Gamma_1 e^{-i\Gamma_1 S_{eq}} & -\Gamma_2 e^{i\Gamma_2 S_{eq}} & \Gamma_2 e^{-i\Gamma_2 S_{eq}} \\ 0 & 0 & (-k+\Gamma_2)e^{i\Gamma^2} & -(k+\Gamma_2)e^{-i\Gamma_2} \end{pmatrix} \begin{pmatrix} c_1 \\ c_2 \\ c_3 \\ c_4 \end{pmatrix} = \begin{pmatrix} 2k \\ 0 \\ 0 \\ 0 \end{pmatrix}$$

where $\Gamma_1=\sqrt{\alpha_1+i\sigma_1}$ and $\Gamma_2=\sqrt{\xi\alpha_1+i\delta\sigma_1}$

$$T_{1eq}(z)=-P\epsilon_1''F(z)+Az+B, \tag{4.43}$$

$$T_{2eq}(z)=-P\frac{\delta}{\lambda}\epsilon_1''G(z)+Cz+D, \tag{4.44}$$

where

$$\begin{aligned} F(z) \;=\; & \frac{|c_1|^2e^{-2Im(\Gamma_1)z}}{4Im(\Gamma_1)^2}-\frac{Re(c_1^*c_2)\cos(2Re(\Gamma_1)z)}{2Re(\Gamma_1)^2} \\ & -\frac{Im(c_1^*c_2)\sin(2Re(\Gamma_1)z)}{2Re(\Gamma_1)^2}+\frac{|c_2|^2e^{2Im(\Gamma_1)z}}{4Im(\Gamma_1)^2} \end{aligned}$$

$$G(z) = \frac{|c_3|^2 e^{-2Im(\Gamma_2)z}}{4Im(\Gamma_2)^2} - \frac{Re(c_3^* c(4))\cos(2Re(\Gamma_2)z)}{2Re(\Gamma_2)^2} - \frac{Im(c_3^* c(4))\sin(2Re(\Gamma_2)z)}{2Re(\Gamma_2)^2} + \frac{|c_4|^2 e^{2Im(\Gamma_2)z}}{4Im(\Gamma_2)^2}$$

$$A = \frac{-\beta(PF(0)+1)+\beta PF(S_{eq})+P\frac{dF}{dz}(0)}{\beta S_{eq}+1} \qquad B = \frac{PF(S_{eq})-S_{eq}P\frac{dF}{dz}(0)+S_{eq}\beta(PF(0)+1)}{\beta S_{eq}+1}$$

$$C = \frac{P\delta/\lambda(G(1)-G(o))+T_{bw}}{1-S_{eq}} \qquad D = \frac{P\delta/\lambda(-G(1)S_{eq}+G(S_{eq}))-T_{bw}S_{eq}}{1-S_{eq}}$$

Starred quantities denote complex conjugates. With these solutions known, the steady-state Stefan condition (4.40) becomes

$$-(P\frac{dF}{dz} + A) + \delta P\frac{dG}{dz} + \lambda C = 0, \tag{4.45}$$

Equation (4.45) constitutes an eigenvalue relation relating the steady front position S_{eq} to the power term P. We can construct steady-state curves relating the steady front position S_{eq} to the microwave power term P using Newton's method. Specifically, we iterate through values of S_{eq} ranging from .02 to .9 and, for each iteration, perform a Newton's iteration on the power level P. Figure 4.3 gives the steady-state positions of the melting front denoted by S_{eq} as a function of power produced by the microwave source for three different Biot numbers. Recall that $T_{bw} = -.5$ represents the value of the temperature T_2 at $z = 1$. The parameter values used in our numerical simulations are those corresponding to water and ice: $\sigma_1 = 80$, $\delta = .01$, $\xi = .04$, $\lambda = 4$, $\mu = 2$. The microwave frequency of consideration is about 2.45 GHZ. It is interesting to note the oscillatory nature of the curves, particularly the curve corresponding to Biot number $\beta = 1$. This curve indicates that for certain power levels, there exist multiple steady-state positions for the melting front. As the Biot number is increased, the steady-state curves become more monotonic. What is interesting here is that these curves all seem to intersect near a particular value of S_{eq}. In fact, this value S_{pivot} can be calculated by considering the case where $P = 0$,

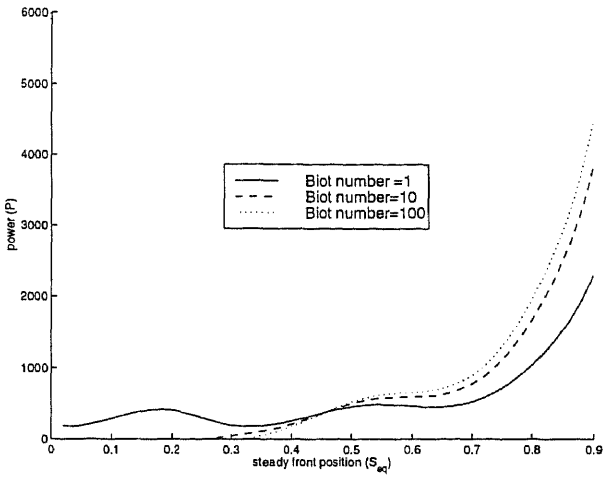

Figure 4.3 Steady-state curves (constant complex permittivity with varying Biot number): $T_{bw} = -.5$; $k = 1$.

which can be thought of as the absence of a microwave source, and by letting β go to infinity or, equivalently, applying a Dirichlet condition on T_1 at $z = 0$ (ie. $T_1 = 1$). The steady-state position of the front for these parameter values is exactly S_{pivot}. Notice that for steady-state front positions $S_{eq} < S_{pivot}$ the power level needed to achieve a given steady-state position decreases with increasing Biot number whereas the power level increases for steady-state positions $S_{eq} > S_{pivot}$. This is due to the fact that at $z = 0$, the boundary condition can assist in the propagation of the melting front up to the value $S_{eq} = S_{pivot}$ so an increase in the Biot number β enhances the propagation. For values $S_{eq} > S_{pivot}$, an increase in the value of the Biot number β can only inhibit the melting front propagation.

Figure 4.4 gives steady curves of S_{eq} vs. P for different boundary values T_{bw} of the temperature T_2. As the boundary temperature decreases, the power levels needed to achieve a steady-state value S_{eq} increase. This is to be expected as the heat flux across the melting front is increased which inhibits the movement of this front. The steady-state curves become less monotonic as the temperature at the boundary is decreased.

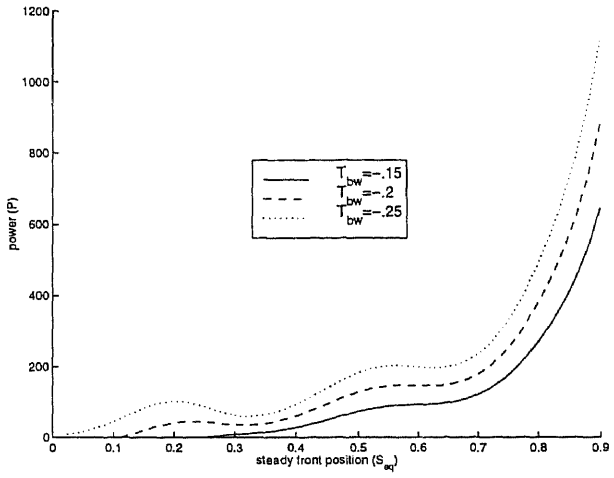

Figure 4.4 Steady-state curves (constant complex permittivity with varying boundary condition): $\beta = 1$; $k = 1$.

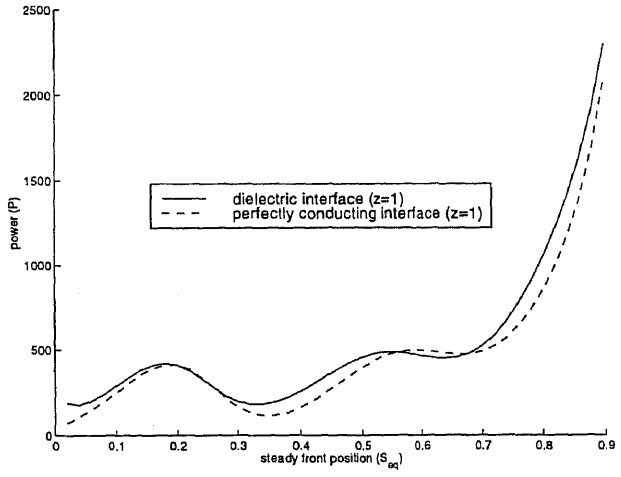

Figure 4.5 Steady-state curves (constant complex permittivity cases): $\beta = 1$; $k = 1$; $T_{bw} = -.5$.

Figure 4.5 compares the steady-state curve for a material layer whose bottom interface is a dielectric interface with a material whose bottom interface is perfectly conducting. Physically, one might think of a material layer resting on a metal surface. Mathematically, the presence of a perfectly conducting surface ($z = 1$) can be modeled by changing the boundary condition (4.27) to $\phi_2 = 0$ at $z = 1$. As can be seen in Figure 4.5, the introduction of a perfectly conducting surface has a noticeable effect on the power necessary to achieve a desired front position S_{eq}.

4.3.2 Asymptotic Limit of Large Stefan Number

In the case of a Large Stefan number L, we can introduce a small parameter ($\epsilon = 1/L$) into the system (4.17-4.28). As will be seen, approximate solutions can be found analytically for the electric fields and the temperature distributions of both the liquid and solid regions of the slab. Consequently, the Stefan condition, at leading order, translates into an ordinary differential equation governing the front position which can be solved using standard numerical techniques. The assumption that L is large motivates the scaling $\tau = \epsilon t$. Substituting this scaling into the system (4.17-4.28) gives the following system:

$$\frac{d^2\phi_1}{dz^2} + k^2(\alpha_1 + i\sigma_1)\phi_1 = 0, \quad 0 < z < S(\tau), \tag{4.46}$$

$$\frac{d^2\phi_2}{dz^2} + k^2(\alpha_1\xi + i\sigma_1\delta)\phi_2 = 0, \quad S(\tau) < z < 1, \tag{4.47}$$

$$\epsilon\mu\lambda\frac{\partial T_1}{\partial \tau} = \frac{\partial^2 T_1}{\partial z^2} + P\beta|\phi_1|^2, \quad 0 < z < S(\tau), \tag{4.48}$$

$$\epsilon\frac{\partial T_2}{\partial \tau} = \frac{\partial^2 T_2}{\partial z^2} + P\frac{\delta}{\lambda}|\phi_2|^2, \quad S(\tau) < z < 1, \tag{4.49}$$

$$\frac{\partial T_1}{\partial z} = \beta(T_1 - 1), \qquad z = 0, \tag{4.50}$$

$$T_1 = T_2 = 0, \qquad z = S(\tau), \tag{4.51}$$

$$T_2 = T_{bw}, \qquad z = 1, \tag{4.52}$$

$$\frac{d\phi_1}{dz} + ik\phi_1 = 2ik, \qquad z = 0, \tag{4.53}$$

$$\phi_1 = \phi_2, \qquad z = S(\tau), \tag{4.54}$$

$$\frac{d\phi_1}{dz} = \frac{d\phi_2}{dz}, \qquad z = S(\tau), \tag{4.55}$$

$$\frac{d\phi_2}{dz} - ik\phi_2 = 0, \qquad z = 1, \tag{4.56}$$

$$-\frac{dT_1}{dz} + \lambda\frac{dT_2}{dz} = \frac{dS}{d\tau}, \qquad z = S(\tau), \tag{4.57}$$

The problem is now posed as one with a small parameter ϵ. We now solve the system by regular perturbation theory. We expand the variables of the system in powers of ϵ as follows:

$$T_1(z,\tau) = T_1^o(z,\tau) + \epsilon T_1^1(z,\tau) + O(\epsilon^2), \tag{4.58}$$

$$T_2(z,\tau) = T_2^o(z,\tau) + \epsilon T_2^1(z,\tau) + O(\epsilon^2), \tag{4.59}$$

$$\phi_1(z,\tau) = \phi_1^o(z,\tau) + \epsilon\phi_1^1(z,\tau) + O(\epsilon^2), \tag{4.60}$$

$$\phi_2(z,\tau) = \phi_2^o(z,\tau) + \epsilon\phi_2^1(z,\tau) + O(\epsilon^2), \tag{4.61}$$

$$S(\tau) = S_o(\tau) + \epsilon S_1(\tau) + O(\epsilon^2), \tag{4.62}$$

Substituting (4.58-4.62) into system (4.46-4.57) and equating like powers of ϵ we attain the successive systems to be solved. Note that functions are represented by a Taylor series in z about S_o at the boundary $z = S$. In general, a function $f(z)$ is expressed as $f(z) = f(S_o) + \frac{df}{dz}(S_o)(z - S_o) + \frac{d^2f}{dz^2}(S_o)(z - S_o)^2 + O(z - S_o)^3$ at z=S. This enables us to deduce boundary conditions at each order of ϵ. To leading order the system is as follows:

$$\frac{d^2\phi_1^0}{dz^2} + k^2(\alpha_1 + i\sigma_1)\phi_1^0 = 0, \quad 0 < z < S_0(\tau), \tag{4.63}$$

$$\frac{d^2\phi_2^0}{dz^2} + k^2(\alpha_1\xi + i\sigma_1\delta)\phi_2^0 = 0, \quad S_0(\tau) < z < 1, \tag{4.64}$$

$$\frac{\partial^2 T_1^0}{\partial z^2} = -P|\phi_1^0|^2, \quad 0 < z < S_0(\tau), \tag{4.65}$$

$$\frac{\partial^2 T_2^0}{\partial z^2} = -P\frac{\delta}{\lambda}\epsilon_2''(T_2^0)|\phi_2^0|^2, \quad S_0(\tau) < z < 1, \tag{4.66}$$

$$\frac{\partial T_1^0}{\partial z} = \beta(T_1^0 - 1), \qquad z = 0, \tag{4.67}$$

$$T_1^0 = T_2^0 = 0, \qquad z = S_0(\tau), \tag{4.68}$$

$$T_2^0 = T - bw, \qquad z = 1, \tag{4.69}$$

$$\frac{d\phi_1^0}{dz} + ik\phi_1^0 = 2ik, \qquad z = 0, \tag{4.70}$$

$$\phi_1^0 = \phi_2^0, \qquad z = S_0(\tau), \tag{4.71}$$

$$\frac{d\phi_1^0}{dz} = \frac{d\phi_2^0}{dz}, \qquad z = S_0(\tau), \tag{4.72}$$

$$\frac{d\phi_2^0}{dz} - ik\phi_2^0 = 0, \qquad z = 1, \tag{4.73}$$

$$-\frac{dT_1^0}{dz} + \lambda\frac{dT_2^0}{dz} = \frac{dS_0}{d\tau}, \qquad z = S_0, \tag{4.74}$$

The $O(\epsilon)$ system is as follows:

$$\frac{d^2\phi_1^1}{dz^2} + k^2(\alpha_1 + i\sigma_1)\phi_1^1 = 0, \quad 0 < z < S_0(\tau), \tag{4.75}$$

$$\frac{d^2\phi_2^1}{dz^2} + k^2(\alpha_1\xi + i\sigma_1\delta)\phi_2^1 = 0, \quad S_0(\tau) < z < 1, \tag{4.76}$$

$$\mu\lambda\frac{\partial T_1^1}{\partial \tau} = \frac{\partial^2 T_1^1}{\partial z^2} + 2P\mathrm{Re}(\phi_1^0\phi_1^{1*}), \quad 0 < z < S_0(\tau), \tag{4.77}$$

$$\frac{\partial T_2^1}{\partial \tau} = \frac{\partial^2 T_2^1}{\partial z^2} + 2P\frac{\delta}{\lambda}\mathrm{Re}(\phi_2^0\phi_2^{1*}), \quad S_0(\tau) < z < 1, \tag{4.78}$$

$$\frac{\partial T_1^1}{\partial z} = \beta T_1^1, \qquad z = 0, \tag{4.79}$$

$$T_1^1(S_0) + \frac{dT_1^0}{dz}(S_0)S_1 = T_2^1(S_0) + \frac{dT_2^0}{dz}(S_0)S_1 = 0, \tag{4.80}$$

$$T_2^1 = 0, \qquad z = 1, \tag{4.81}$$

$$\frac{d\phi_1^1}{dz} + ik\phi_1^1 = 0, \qquad z = 0, \tag{4.82}$$

$$\phi_1^1(S_0) + \frac{d\phi_1^0}{dz}(S_0)S_1 = \phi_2^1(S_0) + \frac{d\phi_2^0}{dz}(S_0)S_1, \tag{4.83}$$

$$\frac{d\phi_1^1}{dz}(S_0) + 2\frac{d^2\phi_1^0}{dz^2}(S_0)S_1 = \frac{d\phi_2^1}{dz}(S_0) + 2\frac{d^2\phi_2^0}{dz^2}(S_0)S_1, \tag{4.84}$$

$$\frac{d\phi_2^1}{dz} - ik\phi_2^1 = 0, \qquad z = 1, \tag{4.85}$$

$$-\left[\frac{dT_1^1}{dz}(S_0) + 2S_1\frac{d^2T_1^0}{dz^2}(S_0)\right] + \lambda\left[\frac{dT_2^1}{dz}(S_0) + 2S_1\frac{d^2T_2^0}{dz^2}(S_0)\right] = \frac{dS_1}{d\tau}, \tag{4.86}$$

Starred quantities denote complex conjugates and Re denotes the real part of the quantity on which it operates. We now restrict our attention to the leading order system, keeping in mind that the higher order systems can be solved to achieve higher order accuracy of the solutions.

Observe that the electric fields ϕ_1^0 and ϕ_2^0 along with temperature distributions T_1^0 and T_2^0, of the leading order system, satisfy the same equations as the steady-state system (4.29-4.39). Hence, $\phi_1^0 = \phi_{1eq}$, $\phi_2^0 = \phi_{2eq}$, $T_1^0 = T_{1eq}$, and $T_2^0 = T_{2eq}$. The system (4.63-4.74) is a quasi-static system in that ϕ_1^0, ϕ_2^0, T_1^0 and T_2^0 depend parametrically on the front position $S_0(\tau)$. Since the temperature and electric fields of both regions are known functions of $S_0(\tau)$, the Stefan condition (4.74) becomes the governing ordinary differential equation for the leading order melting front trajectory

$$-(P\frac{dF}{dz} + A) + \delta P\frac{dG}{dz} + \lambda C = \frac{dS_o}{d\tau}, \tag{4.87}$$

Equation (4.87) and an initial condition on S_o constitute an initial value problem to be solved. Solutions are found using a Matlab ordinary differential equations solver.

Figure 4.6 gives plots for the position of the melting front $S(t)$ vs. its rate of change $S'(t)$ in the limit of large Stefan number ($L >> 1$). The plots are given for two different power levels. As can be seen for $P = 400$, there exist three steady-state positions for the melting front. The equilibrium points $S = .15$ and $S = .47$ are stable nodes while $S = .21$ is an unstable node. If the power P is increased by 40 units the number of equilibrium points is reduced to one. This point $S = .48$ is a stable node. So, for a relatively small change in the power P, the dynamical nature of the system (4.104-4.115) is altered significantly.

Figure 4.10 shows the front trajectory in time for $L >> 1$.

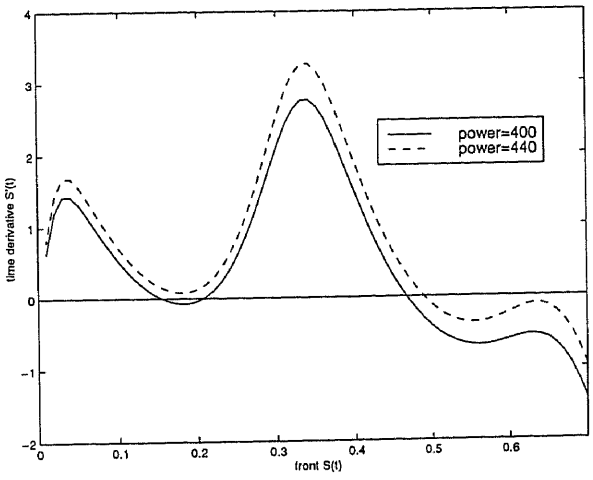

Figure 4.6 Melting front position S vs. derivative S': $\beta = 1$; $k = 1$.

4.4 The Case of Temperature Dependent Dielectric Attributes

4.4.1 Steady-State Solutions

The calculation of the steady-state solutions in this case where the dielectric attributes of a material depend on temperature, is more complicated than the calculation for the case of constant dielectric properties. This is due to the fact that the temperature fields and the electric fields of the liquid and solid regions are now coupled together. We will use the same notation to denote the equilibrium solutions as we did in the previous section. Taking the time derivatives of the system (4.17-4.28) to be zero, we arrive at the steady-state system:

$$\frac{d^2\phi_{1eq}}{dz^2} + k^2(\alpha_1\epsilon_1'(T_{1eq}) + i\sigma_1\epsilon_1''(T_{1eq}))\phi_{1eq} = 0, \quad 0 < z < S_{eq}, \tag{4.88}$$

$$\frac{d^2\phi_{2eq}}{dz^2} + k^2(\alpha_1\xi\epsilon_2'(T_{2eq}) + i\sigma_1\delta\epsilon_2''(T_{2eq}))\phi_{2eq} = 0, \quad S_{eq} < z < 1, \tag{4.89}$$

$$\frac{\partial^2 T_{1eq}}{\partial z^2} = -P\epsilon_1''(T_{1eq})|\phi_{1eq}|^2, \quad 0 < z < S_{eq}, \tag{4.90}$$

$$\frac{\partial^2 T_{2eq}}{\partial z^2} = -P\frac{\delta}{\lambda}\epsilon_2''(T_{2eq})|\phi_{2eq}|^2, \quad S_{eq} < z < 1, \tag{4.91}$$

$$\frac{\partial T_{1eq}}{\partial z} = \beta(T_1 - 1), \qquad z = 0, \tag{4.92}$$

$$T_{1eq} = T_{2eq} = 0, \qquad z = S_{eq}, \tag{4.93}$$

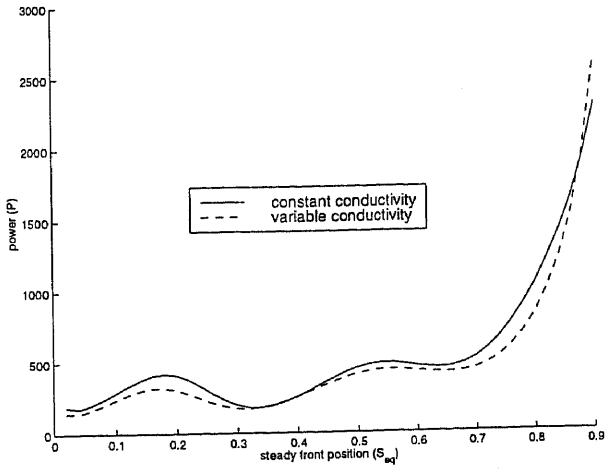

Figure 4.7 Steady-state curves (constant and variable complex permittivity cases): $\beta = 1$; $k = 1$; $T_{bw} = -.5$.

$$T_{2eq} = T_{bw}, \qquad z = 1, \tag{4.94}$$

$$\frac{d\phi_{1eq}}{dz} + ik\phi_{1eq} = 2ik, \qquad z = 0, \tag{4.95}$$

$$\phi_{1eq} = \phi_{2eq}, \qquad z = S_{eq}, \tag{4.96}$$

$$\frac{d\phi_{1eq}}{dz} = \frac{d\phi_{2eq}}{dz}, \qquad z = S_{eq}, \tag{4.97}$$

$$\frac{d\phi_{2eq}}{dz} - ik\phi_{2eq} = 0, \qquad z = 1, \tag{4.98}$$

The nondimensional Stefan condition is:

$$-\frac{dT_{1eq}}{dz} + \lambda\frac{dT_{2eq}}{dz} = 0, \qquad z = S_{eq}, \tag{4.99}$$

The problem posed here is an eigenvalue problem relating the steady-state front position S_{eq} to the power term P. The steady-state temperatures, electric fields and melting front position are found by implementing a shooting method on the system (4.88-4.99). Specifically guesses are made for $\phi_{1eq}(0)$, $T_{1eq}(0)$ and the power P. So, for a given value of the parameter S_{eq} the shooting method converges to a certain value of P. To solve this system we employ a Newton Raphson method in conjunction with a Matlab ODE solver routine.

Figure 4.7 displays the steady-state curve with $T_{bw} = -.5$ for the cases of temperature dependent dielectric permittivity and constant dielectric permittivity. The nonmonotonic behavior of both curves is very pronounced. There is a significant difference in the steady-state power levels predicted by the curves, which demonstrates the importance of including the temperature dependence of the complex dielectric permittivity in the mathematical model.

4.5 A Fixed Front Method For Tracking the Moving Boundary

The main idea of the front fixing method is to make a transformation of variables in order to transform the moving boundary value problem (4.17-4.28) into a fixed boundary value problem where the boundary $S(t)$ will now enter into the partial differential equations of the system. For $S(t) < z < 1$, we let $\zeta = (z - S(t))/(1 - S(t))$. For $0 < z < S(t)$, we let $\eta = z/S(t)$. With these transformations, the region $S(t) < z < 1$ is mapped into $0 < \zeta < 1$, and $0 < z < S(t)$ is mapped into $0 < \eta < 1$. The melting front is at $\zeta = 0$, $\eta = 1$. The transformation of the time and space derivatives in t and z are as follows:

$$\frac{\partial}{\partial t} \to \frac{\partial}{\partial t} + \frac{dS}{dt}\frac{\zeta - 1}{1 - S}\frac{\partial}{\partial \zeta}, \quad 0 < \zeta < 1, \tag{4.100}$$

$$\frac{\partial}{\partial z} \to \frac{1}{1 - S}\frac{\partial}{\partial \zeta}, \quad 0 < \zeta < 1, \tag{4.101}$$

$$\frac{\partial}{\partial t} \to \frac{\partial}{\partial t} - \frac{dS}{dt}\frac{\eta}{S}\frac{\partial}{\partial \eta}, \quad 0 < \eta < 1, \tag{4.102}$$

$$\frac{\partial}{\partial z} \to \frac{1}{S}\frac{\partial}{\partial \eta}, \quad 0 < \eta < 1, \tag{4.103}$$

With these transformations the system (4.17-4.28) becomes:

$$\frac{d^2\phi_1}{d\eta^2} + S^2k^2(\alpha_1\epsilon_1'(T_1) + i\sigma_1\epsilon_1''(T_1))\phi_1 = 0, \quad 0 < \eta < 1, \tag{4.104}$$

$$\frac{d^2\phi_2}{d\zeta^2} + (1 - S)^2k^2(\alpha_1\xi\epsilon_2'(T_2) + i\sigma_1\delta\epsilon_2''(T_2))\phi_2 = 0, \quad 0 < \zeta < 1, \tag{4.105}$$

$$\mu\lambda(\frac{\partial T_1}{\partial t} - \frac{dS}{dt}\frac{1}{S}\eta\frac{\partial T_1}{\partial \eta}) = \frac{1}{S^2}\frac{\partial^2 T_1}{\partial \eta^2} + P\epsilon_1''(T_1)|\phi_1|^2, \quad 0 < \eta < 1, \tag{4.106}$$

$$\frac{\partial T_2}{\partial t} + \frac{dS}{dt}\frac{\zeta - 1}{1 - S}\frac{\partial T_2}{\partial \zeta} = \frac{1}{(1-S)^2}\frac{\partial^2 T_2}{\partial \zeta^2} + P\frac{\delta}{\lambda}\epsilon_2''(T_2)|\phi_2|^2, \quad 0 < \zeta < 1, \tag{4.107}$$

$$\frac{\partial T_1}{\partial \eta} = S\beta(T_1 - 1), \qquad \eta = 0, \tag{4.108}$$

$$T_1(\eta) = T_2(\zeta) = 0, \qquad \zeta = 0,\ \eta = 1, \tag{4.109}$$

$$T_2 = T_{bw}, \qquad \zeta = 1, \tag{4.110}$$

$$\frac{d\phi_1}{d\eta} + ikS\phi_1(\eta) = 2ikS, \qquad \eta = 0, \tag{4.111}$$

$$\phi_1(\eta) = \phi_2(\zeta), \qquad \zeta = 0,\ \eta = 1, \tag{4.112}$$

$$(1 - S)\frac{d\phi_1}{d\eta} = S\frac{d\phi_2}{d\zeta}, \qquad \zeta = 0,\ \eta = 1, \tag{4.113}$$

$$\frac{d\phi_2}{d\zeta} - ik(1 - S)\phi_2 = 0, \qquad \zeta = 1, \tag{4.114}$$

$$-\frac{dT_1}{d\eta}\frac{1}{S} + \lambda\frac{dT_2}{d\zeta}\frac{1}{1 - S} = L\frac{dS}{dt}, \qquad \zeta = 0,\ \eta = 1, \tag{4.115}$$

This is the full nondimensional system to be analyzed.

4.5.1 Numerical Implementation

The importance of making the transformation to fix the boundaries is that a finite difference scheme can be employed to solve the system without the need to adapt the mesh in space to accommodate the moving boundary. A main objective in this work is to track the melting front S with time. Since the problem is one dimensional, the trajectory of the front is expected to be smooth with time. Implicit finite difference schemes are generally efficient methods to track this front. Note that there are two boundary value problems to be solved; one for the liquid region and one for the solid region. We employ a Crank Nicolsen implicit scheme for each region with explicit reference given to the moving front S. The intervals $0 < \eta < 1$ and $0 < \zeta < 1$ are discretized into N subintervals or $N + 1$ nodal points where i denotes the index to each of these points. Here $\triangle z = 1/N$ denotes the spatial step size and $\triangle t$ denotes the temperal step size, and j denotes the index in time t.

4.5.2 The Case of Constant Dielectric Properties (General Stefan Number)

With the assumption of constant dielectric attributes, ϵ_1', ϵ_2', ϵ_1'',and ϵ_2'' are unity. Observe that equations (4.104) and (4.105) are decoupled from the heat equations in the solid and liquid regions. Using these, together with the boundary conditions (4.111-4.114), we can deduce an exact solution for the electric fields in both the liquid and solid portions of the material. The solutions are given as:

$$\phi_1 = Ae^{ikS\Gamma_1\eta} + Be^{-ikS\Gamma_1\eta}, \tag{4.116}$$

$$\phi_2 = Ce^{ik(1-S)\Gamma_2\zeta} + De^{-ik(1-S)\Gamma_2\zeta}, \tag{4.117}$$

where

$$\Gamma_1 = \sqrt{\alpha_1 + i\sigma_1} \qquad \Gamma_2 = \sqrt{\xi\alpha_1 + i\delta\sigma_1}$$

$$B = -\frac{2}{\Gamma_1 - 1} + A\frac{\Gamma_1+1}{\Gamma_1-1} \qquad D = C\frac{\Gamma_2-1}{\Gamma_2+1}e^{2ik(1-S)\Gamma_2}$$

A and C are determined from the following system:

$$\begin{pmatrix} F_{11} & F_{12} \\ F_{21} & F_{22} \end{pmatrix} \begin{pmatrix} A \\ C \end{pmatrix} = \begin{pmatrix} b \\ -b \end{pmatrix}$$

where

$$F_{11} = e^{ikS\Gamma_1} + \frac{\Gamma_1+1}{\Gamma_1-1}e^{-ikS\Gamma_1} \qquad F_{21} = e^{ikS\Gamma_1} - \frac{\Gamma_1+1}{\Gamma_1-1}e^{-ikS\Gamma_1}$$

$$F_{12} = -(1 + e^{2ik(1-S)\Gamma_2}\frac{\Gamma_2-1}{\Gamma_2+1}) \qquad F_{22} = -\frac{\Gamma_2}{\Gamma_1}(1 - \frac{\Gamma_2-1}{\Gamma_2+1}e^{2ik(1-S)\Gamma_2})$$

$$b = 2e^{-ikS\Gamma_1}\frac{1}{\Gamma_1-1}$$

With analytical solutions of the electric fields given, the semi- implicit Crank Nicolson discretizations need to be carried out only on the energy equations in each of the respective (liquid/solid) regions. The discretization of the system (4.106)-(4.107) is:

$$T^{j+1}_{1,i-1}A_1 + T^{j+1}_{1,i}B_1 + T^{j+1}_{1,i+1}C_1 = -T^{j}_{1,i-1}A_1 + T^{j}_{1,i}D_1 - T^{j}_{1,i+1}C_1 + P|\phi_{1i}|^2, \tag{4.118}$$

$$T^{j+1}_{2,i-1}A_2 + T^{j+1}_{2,i}B_2 + T^{j+1}_{2,i+1}C_2 = -T^{j}_{2,i-1}A_2 + T^{j}_{2,i}D_2 - T^{j}_{2,i+1}C_2 + P\frac{\delta}{\lambda}|\phi_{2i}|^2, \quad (4.119)$$

where the discrete representations for the spatial derivatives and the time derivative are:

$$\frac{\partial f}{\partial z} = \frac{f_{i+1}-f_{i-1}}{2\triangle z} \qquad \frac{\partial^2 f}{\partial z^2} = \frac{f_{i-1}-2f_i+f_{i+1}}{(\triangle z)^2} \qquad \frac{\partial f}{\partial t} = \frac{f^{j+1}-f^j}{\Delta t}$$

The coefficients are given as:

$$A_1 = \mu\lambda S\frac{dS}{dt}\frac{\Delta t}{\Delta z} - 2\frac{\Delta t}{(\Delta z)^2} \qquad B_1 = 4\left(\mu\lambda S^2 + \frac{\Delta t}{(\Delta z)^2}\right)$$

$$C_1 = -\mu\lambda S\frac{dS}{dt}\frac{\Delta t}{\Delta z} - 2\frac{\Delta t}{(\Delta z)^2} \qquad D_1 = 4\left(\mu\lambda S^2 - \frac{\Delta t}{(\Delta z)^2}\right)$$

$$A_2 = (1-S)\frac{dS}{dt}(\zeta-1)\frac{\Delta t}{\Delta z} - 2\frac{\Delta t}{(\Delta z)^2} \qquad B_2 = 4\left((1-S)^2 + \frac{\Delta t}{(\Delta z)^2}\right)$$

$$C_2 = -(1-S)\frac{dS}{dt}(\zeta-1)\frac{\Delta t}{\Delta z} - 2\frac{\Delta t}{(\Delta z)^2} \qquad D_2 = 4\left((1-S)^2 - \frac{\Delta t}{(\Delta z)^2}\right)$$

(4.118) and (4.119) hold for $2 \le i \le N$. For $i = 1$, boundary conditions (4.108) and (4.109) yield the following discrete equations:

$$\begin{aligned} T^{j+1}_{1,1}(B_1 - 2\triangle z S\beta A_1) + T^{j+1}_{1,2}(A_1 + C_1) \;&=\; T^{j}_{1,1}(D_1 + 2\triangle z S\beta A_1) \\ &\quad -T^{j}_{1,2}(A_1 + C_1) + P|\phi_1|^2, \end{aligned} \quad (4.120)$$

$$T_{2,1} = 0 \quad (4.121)$$

The centered difference formula for the first derivative introduces a fictitious point $T^j_{1,0}$ at the boundary $\eta = 0$. This point can be represented in terms of $T^j_{1,1}$ and $T^j_{1,2}$ through the use of the mixed boundary condition (4.108). Observe that the centered difference representation for first derivatives has $O((\triangle z)^2)$ accuracy whereas the one-sided representation has $O(\triangle z)$ accuracy. For $i = N+1$, boundary conditions (4.109) and (4.110) yield:

$$T^j_{1,N+1} = 0, \quad (4.122)$$

$$T^j_{2,N+1} = T_{bw}, \quad (4.123)$$

Equations (4.118-4.123) represent the closed discrete system to be solved for both regions (liquid and solid). In each region, the discrete system is set up as a tridiagonal matrix system to be solved.

4.5.3 The Case of Temperature Dependent Dielectric Properties (General Stefan Number)

In general, the dielectric attributes of a material do depend on temperature. In this case the system (4.104-4.115) becomes more complicated to solve as equations (4.104) and (4.105) governing the electric fields in the liquid and solid regions respectively are now coupled to the energy equations (4.106) and (4.107). We must therefore resort to numerical methods to solve for these fields along with the temperature distributions. We use Richmeyer's Method (see Smith G. (1993)) in dealing with the nonlinear terms involving the temperature distributions of the liquid and solid regions. We now discuss the philosophy of the method.

In discretizing the system (4.104-4.115), we use the same finite difference representations for the space and time derivatives as before. Notice that (4.106) and (4.107) contain nonlinear terms in T_1 and T_2 respectively. In general, we can expand a nonlinear term (say $F(T)$) as $F(T) = F(T^j) + \frac{dF(T^j)}{dT}(T - T^j) + O(\triangle T^2)$. This is just the Taylor series representation of F about T^j. Since $\triangle T = T^{j+1} - T^j$ is small for small time steps, the Taylor series expansion is a good approximation. We can now rewrite $F(T)$ as $F(T^j) + \frac{dF(T^j)}{dT}(T^{j+1} - T^j)$. Using this finite difference representation for the nonlinear terms of (4.106-4.107) along with the finite difference representations given previously yields the following finite difference scheme:

$$\phi_{1,1}(E_1 + 2i\triangle zkS) + 2\phi_{1,2} = 4ikS, \tag{4.124}$$

$$\phi_{1,i-1} + \phi_{1,i}E_1 + \phi_{1,i+1} = 0, \qquad 2 \leq i \leq N, \tag{4.125}$$

$$\phi_{1,N+1} = \phi_{2,1}, \tag{4.126}$$

$$\phi_{1,N+1} - \phi_{1,N} = \phi_{2,2} - \phi_{2,1}, \tag{4.127}$$

$$\phi_{2,i-1} + \phi_{2,i}E_2 + \phi_{2,i+1} = 0, \qquad 2 \le i \le N, \tag{4.128}$$

$$\phi_{2,N+1}(E_2 - 2i\triangle zk(1-S)) + 2\phi_{2,N} = 0, \tag{4.129}$$

$$\begin{aligned} T_{1,1}^{j+1}(B_1 + F_{1,1} - 2\triangle zS\beta A_1) + T_{1,2}^{j+1}(A_1 + C_1) &= T_{1,1}^{j}(D_1 + F_{1,1} + 2\triangle zS\beta A_1) \\ &\quad -T_{1,2}^{j}(A_1 + C_1) \\ &\quad +P\epsilon_1''(T_{1,1}^{j})|\phi_{1,1}|^2, \end{aligned} \tag{4.130}$$

$$\begin{aligned} T_{1,i-1}^{j+1}A_1 + T_{1,i}^{j+1}(B_1 + F_{1,i}) + T_{1,i+1}^{j+1}C_1 &= -T_{1,i-1}^{j}A_1 + T_{1,i}^{j}(D_1 + F_{1,i}) \\ &\quad -T_{1,i+1}^{j}C_1 + P\epsilon_1''(T_{1,i}^{j})|\phi_{1,i}|^2, \\ &\quad 2 \le i \le N, \end{aligned} \tag{4.131}$$

$$T_{1,N+1} = 0, \tag{4.132}$$

$$T_{2,1} = 0, \tag{4.133}$$

$$\begin{aligned} T_{2,i-1}^{j+1}A_2 + T_{2,i}^{j+1}(B_2 + F_{2,i}) + T_{2,i+1}^{j+1}C_2 &= -T_{2,i-1}^{j}A_2 + T_{2,i}^{j}(D_2 + F_{2,i}) \\ &\quad -T_{2,i+1}^{j}C_2 + P\frac{\delta}{\lambda}\epsilon_2''(T_{2,i}^{j})|\phi_{2,i}|^2, \\ &\quad 2 \le i \le N, \end{aligned} \tag{4.134}$$

$$T_{2,N+1} = T_{bw}, \tag{4.135}$$

where

$$E_1 = -2 + (\triangle z)^2S^2k^2(\alpha_1\epsilon_1'(T_{1,i}^{j}) + i\sigma_1\epsilon_1''(T_{1,i}^{j})) \qquad F_{1,i} = -2\triangle tP\tfrac{d}{dT}\epsilon_1''(T_{1,i}^{j})|\phi_{1,i}|^2$$

$$E_2 = -2 + (\triangle z)^2(1-S)^2k^2(\xi\alpha_1\epsilon_2'(T_{2,i}^{j}) + i\delta\sigma_1\epsilon_2''(T_{2,i}^{j})) \qquad F_{2,i} = -2\triangle tP\tfrac{d}{dT}\epsilon_2''(T_{2,i}^{j})|\phi_{2,i}|^2$$

As in the case of constant complex permittivity, the problem is posed as tridiagonal matrix system to be solved in the liquid and solid regions of the material. The tridiagonal entries of the matrix are different due to the nonlinear terms involving the temperature field for each region.

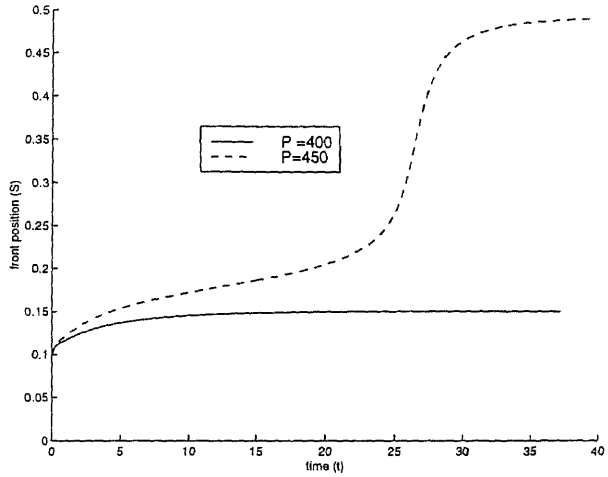

Figure 4.8 Melting front position S vs. time t (constant complex dielectric permittivity): $\beta = 1$; $k = 1$.

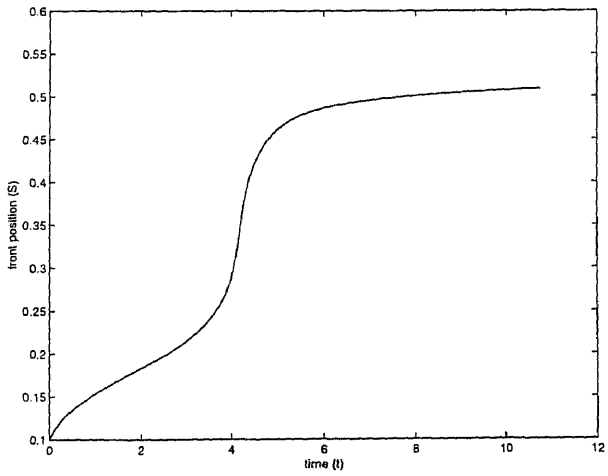

Figure 4.9 Melting front position S vs. time t (temperature dependent complex dielectric permittivity): P=400; $\beta = 1$; $k = 1$.

Figure 4.8 gives the trajectory of the melting front in time for $P = 400$ and $P = 450$. Here the complex dielectric permittivity is assumed constant. As suggested by the corresponding steady-state curves, the melting front for $P = 400$ propagates out to $S_{eq} = .15$. But, for $P = 450$ the front moves much farther before coming to rest ($S_{eq} = .49$). Figure 4.9 gives the trajectory of the melting front in time for $P = 400$. Here the temperature dependence of the complex dielectric permittivity is taken into account. The model incorporating this temperature dependence predicts that melting front front will propagate much farther to a value $S_{eq} = .51$ as compared with the constant permittivity model.

Figure 4.10 gives plots of the trajectory of the melting front position $S(\tau)$ vs. τ for the case of constant complex dielectric permittivity. The solid curve denotes the trajectory calculated using the leading order asymptotic result for the large Stefan number limit ($L \to \infty$). The dashed curve shows the trajectory for $L = 33$ and the dotted curve gives the trajectory for $L = 100$. These curves are calculated using the finite difference routine discussed. Note that as the Stefan number L is increased, the trajectories given by the finite difference code converge to the asymptotic result. In calculating the melting front trajectory, it is far more efficient to employ asymptotic approximations when $L >> 1$ than it is to use the finite difference algorithm in that the computational run time can be reduced dramatically. Note that for $L >> 1$ the asymptotic approximation serves as a good check on the finite difference algorithm.

Figure 4.11 compares the melting front trajectory in time for a layer of material whose bottom interface is a dielectric interface, with a material whose bottom interface is prefectly conducting. For the power setting studied here ($P = 600$), the melting front propagates faster and farther for the case of a perfectly conducting interface at ($z = 1$) than it does for the case of a dielectric interface at ($z = 1$).

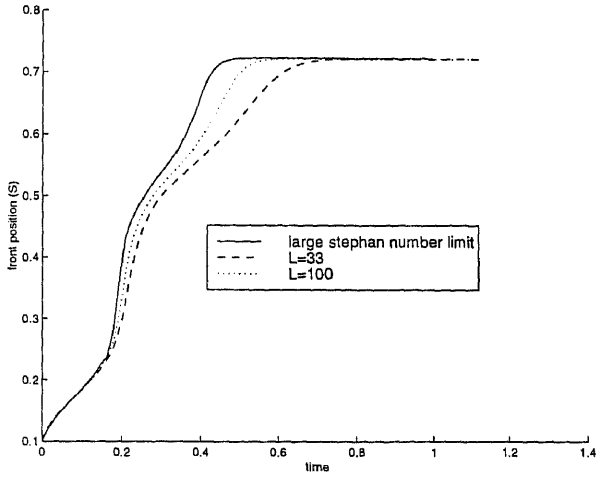

Figure 4.10 Melting front position S vs. time τ: $P = 600$; $\beta = 1$; $k = 1$; $T_{bw} = -.5$.

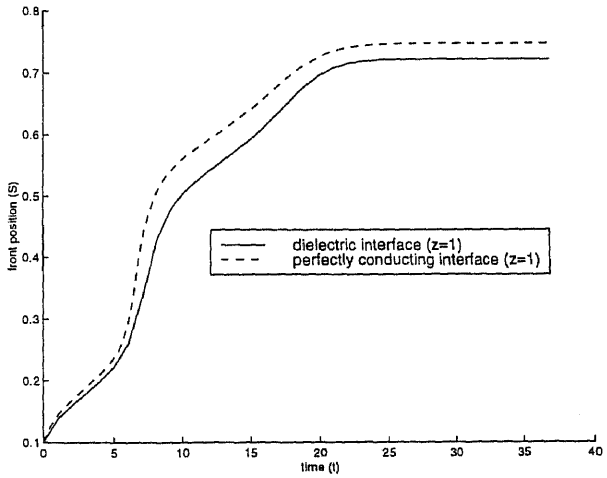

Figure 4.11 Melting front position S vs. time t: $P = 600$; $\beta = 1$; $k = 1$; $T_{bw} = -.5$.

4.6 Discussion

The model posed gives some physical insight into the melting of solids that was not known *a priori*. For example, the numerical experiments conducted suggest that the final resting position of the melting front depends, in a highly nonlinear manner, on the power. If it is desirable to melt only a certain portion of the solid material, the model suggests how the power should be controlled in order to achieve the desired steady-state melting front position. For example, the steady-state curve (4.7) implies that given an initial melting front position $S_{init} = .1$, in order to move the front out to (say $S_{eq} = .4$), the power term P should increase beyond $P_{crit} = 408$, and then decreased to a value of about $P = 300$. This is an interesting hysteresis phenomenon. That is, the trajectory of S_{eq} obtained by increasing P from a value less than P_{crit} to a value greater than P_{crit}, is not the same as that obtained when decreasing P from a level greater than P_{crit} to a level less than P_{crit}. Mathematically, when P starts out below P_{crit}, S_{eq} tracks one stable branch of the steady-state curve. Once P exceeds $P = P_{crit}$ it jumps to another stable branch of this curve, and reducing P forces S_{eq} to continue along this new stable branch. Note that in a transient problem, given the initial conditions, the times taken to reach a given state differ depending on the branch traversed. This provides useful quantitative information for applications.

As was seen in Figure 4.11, the amount of power necessary to achieve a desired melting front position can be reduced, in many cases, by introducing a reflective surface at the bottom of the material layer. In commercial processes where it is desirable to use the least amount of power possible in processing a material, the results discussed may have potential applications. In estimating power levels necessary to achieve a desired steady front position, it is important, for certain materials, to account for the temperature dependence of the complex dielectric permittivity.

APPENDIX A

THE METHOD OF MULTIPLE SCALES

We present the full equations in dimensional form :

$$\triangle \mathbf{E}' - \nabla(\nabla \cdot \mathbf{E}') = \mu_o \left[\frac{\partial^2}{\partial t'^2}(\epsilon_r(T)\mathbf{E}') + \frac{\partial}{\partial t'}(\sigma(T')\mathbf{E}') \right] \tag{A.1}$$

$$\rho c_p [\frac{\partial T'}{\partial t'} + (\mathbf{u}' \cdot \nabla)T'] = k_t \triangle T' + \frac{\sigma}{2}|\mathbf{E}'|^2 \tag{A.2}$$

$$\frac{\partial \mathbf{u}'}{\partial t'} + (\mathbf{u}' \cdot \nabla)\mathbf{u}' = \frac{-\nabla P'}{\rho_o} - \rho/\rho_o g + \nu \triangle \mathbf{u}' \tag{A.3}$$

$\mathbf{u}' = (u_1', u_2', u_3')$ represents the velocity vector field, T' is the temperature P' is the pressure and $\mathbf{E}'$ is the electric field. μ_0, ϵ_r and σ are magnetic permeability, the permittivity and the conductivity, respectively, of the dielectric. k_t is the thermal conductivity. ρ is the density of the dielectric and ρ_0 is the reference density at the ambient temperature. ν is the kinematic viscosity of media.

In the above system we recognize that there are two time scales present in the physical problem. The oscillatory time of the electric field and the diffusive time for the temperature. In order that we may study the thermo-dynamical aspects of the physical system we wish to study the long time (diffusive time) behavior of the system. To do this we scale the dimensional oscillatory time (say t_1) w.r.t. the electromagnetic wave frequency and note that the slow time variable (say τ) $= \delta t_1$ where $\delta = \kappa/(\omega d^2)$ is a small parameter. Note $\frac{d}{dt} = \frac{\partial}{\partial t} + \frac{\partial}{\partial \tau}\frac{d\tau}{dt}$ We introduce the following scalings to nondimensionalize A.1-A.3:

$$\mathbf{x} = \mathbf{x}'/d, \quad t = \omega t', \quad \mathbf{u} = d\mathbf{u}'/\kappa, \quad P = d^2/(\kappa^2 \rho_o)P'$$

$$\theta = (-1 + \frac{\theta'}{\theta_o}), \quad \mathbf{E} = \mathbf{E}'/E_0$$

$$R = (\alpha g d^3 \theta_o)/(\kappa\nu), \quad Pr = \nu/\kappa, \quad \beta = hd/k_t, \quad \chi = \sigma_o |E_o|^2 d^2/(2k_t\theta_o). \tag{A.4}$$

We arrive at the following nondimensional system with the small parameter (δ):

$$\triangle \mathbf{E} - \nabla(\nabla \cdot \mathbf{E}) = k^2 \left[\frac{\partial^2}{\partial t^2}(\epsilon_r \mathbf{E}) + \frac{\sigma_o}{\epsilon_o \omega} \frac{\partial}{\partial t}(f(T)\mathbf{E}) \right] \tag{A.5}$$

$$\frac{\partial T}{\partial t} + \delta(\mathbf{u} \cdot \nabla)T] = \delta[\triangle T + \chi f(T)|\mathbf{E}|^2] \tag{A.6}$$

$$\frac{\partial \mathbf{u}}{\partial t} + \delta(\mathbf{u} \cdot \nabla)\mathbf{u} = \delta(-\nabla p - (d^3/\kappa^2 g + RprT)\mathbf{k} + pr\triangle \mathbf{u}) \tag{A.7}$$

We now perform asymptotics on the above system to attain a leading order system in δ that is uniformly valid for all time. Let $\mathbf{u} = \mathbf{u}_o + \delta \mathbf{u}_1$, $\mathbf{E} = \mathbf{E}_o + \delta \mathbf{E}_1$ and $T = T_o + \delta T_1$.

The leading order system:

$$\triangle \mathbf{E}_o - \nabla(\nabla \cdot \mathbf{E}_o) = k^2 \left[\frac{\partial^2}{\partial t^2}(\epsilon_r \mathbf{E}_o) + \frac{\sigma_o}{\epsilon_o w} \frac{\partial}{\partial t}(f(T_o)\mathbf{E}_o) \right] \tag{A.8}$$

$$\frac{\partial T_o}{\partial t} = 0 \tag{A.9}$$

$$\frac{\partial \mathbf{u}_o}{\partial t} = 0 \tag{A.10}$$

$$\nabla \cdot \mathbf{u} = 0 \tag{A.11}$$

Hence $T_o = g(\mathbf{x}, \tau)$, $\mathbf{u}_o = \mathbf{h}(\mathbf{x}, \tau)$ and $\mathbf{E}_o = L(\tau)\hat{\mathbf{E}}_o(\mathbf{x})e^{i\omega t_1}$ are solutions.

let $L = \frac{\sigma}{\omega \epsilon_o} \frac{\partial}{\partial t}(f'(T_o)T_1 \mathbf{E}_o) + \frac{\partial^2}{\partial t^2}(\epsilon_r'(T_o)T_1 \mathbf{E}_o)$

$$M = \frac{\partial^2}{\partial t_1 \partial \tau}(\epsilon_r(T_o)\mathbf{E}_o) + \frac{\sigma}{\omega \epsilon_o} \frac{d}{d\tau}(f(T_o)\mathbf{E}_o)$$

The $O(\delta)$ system:

$$\triangle \mathbf{E}_1 - \nabla(\nabla \cdot \mathbf{E}_1) = k^2 [\frac{\partial^2}{\partial t^2}(\epsilon_r \mathbf{E}_1) + \frac{\sigma_o}{\omega \epsilon_o} \frac{\partial}{\partial t}(f(T_o)\mathbf{E}_1) + L + M] \tag{A.12}$$

$$\frac{\partial T_1}{\partial t} = -(\mathbf{u}_o \cdot \nabla)T_o - \frac{\partial T_o}{\partial \tau} + \triangle T_o + \chi f(T_o)|\mathbf{E}_o|^2 \tag{A.13}$$

$$\frac{\partial \mathbf{u}_1}{\partial t} = -(\mathbf{u}_o \cdot \nabla)\mathbf{u}_o - \frac{\partial \mathbf{u}_o}{\partial \tau} + (-\nabla p - (d^3/\kappa^2 g + RprT)\mathbf{k} + pr\triangle \mathbf{u}_o) \tag{A.14}$$

$$\nabla \cdot \mathbf{u}_1 = 0 \tag{A.15}$$

Integrating A.13 with respect to the fast time t and letting t go to infinity we get:

$$-(\mathbf{u}_o \cdot \nabla)T_o - \frac{\partial T_o}{\partial \tau} + \triangle T_o + \chi f(T_o) \lim_{t\to\infty} \frac{1}{t}\int_0^t |\mathbf{E}_o|^2 = 0 \tag{A.16}$$

note that $u_1 = \mathbf{\Gamma}(\mathbf{x}, \tau)t$ where $\mathbf{\Gamma}$ denotes the right hand side of A.14. In order for our leading order expansion to be uniformly valid over all time we require that $\mathbf{\Gamma}$ equal zero.

APPENDIX B

DERIVATION OF EQUATIONS GOVERNING "COMPLEX ELECTRIC FIELD"

From Maxwell's equations we deduce the following general equation governing the behavior of the electric field within in dielectric medium.

$$\triangle \mathbf{E} - \nabla(\nabla \cdot \mathbf{E}) = \frac{1}{c}\left[\frac{\partial^2}{\partial t^2}(\epsilon_r(T)\mathbf{E}) + \frac{\partial}{\partial t}(\frac{\sigma(T)}{\epsilon_o}\mathbf{E})\right] \tag{B.1}$$

From our two-timing analysis we determined that σ and ϵ_r only evolve on the slow time scale τ. Hence, we can place these variables out of the time derivative operators to get:

$$\triangle \mathbf{E} - \nabla(\nabla \cdot \mathbf{E}) = \frac{1}{c}\left[(\epsilon_r(T)\frac{\partial^2}{\partial t^2}\mathbf{E}) + \frac{\sigma(T)}{\epsilon_o}\frac{\partial}{\partial t}(\mathbf{E})\right] \tag{B.2}$$

We expect the electric field to have a time harmonic behavior so the solution is assumed of the form:

$$\mathbf{E}(\mathbf{x}, t) = \mathbf{A}(\mathbf{x})sin(\omega t) + \mathbf{B}(\mathbf{x})cos(\omega t) \tag{B.3}$$

Substituting this expression for $\mathbf{E}$ into B.2 and equating sine and cosine terms yields two equations:

$$\triangle \mathbf{A} - \nabla(\nabla \cdot \mathbf{A}) = \frac{1}{c}\left[(-\epsilon_r(T)\omega^2\mathbf{A}) - \omega\frac{\sigma(T)}{\epsilon_o}(\mathbf{B})\right] \tag{B.4}$$

$$\triangle \mathbf{B} - \nabla(\nabla \cdot \mathbf{B}) = \frac{1}{c}\left[(-\epsilon_r(T)\omega^2\mathbf{B}) + \omega\frac{\sigma(T)}{\epsilon_o}(\mathbf{A})\right] \tag{B.5}$$

Let $\mathbf{e_o} = A + iB$. Adding i times B.5 to B.4 gives:

$$\triangle \mathbf{e_o} - \nabla(\nabla \cdot \mathbf{e_o}) = -k^2\left[\epsilon_r(T)\mathbf{e_o} + i\epsilon_r''(T)\mathbf{e_o}\right] \tag{B.6}$$

where $\epsilon_r''(T) = \frac{\sigma(T)}{\epsilon_o \omega}$ note the physical electric field $\mathbf{E}$ is represented in terms of $\mathbf{e_o}$ as $\mathbf{E} = \text{real}(\mathbf{e_o} e^{-i\omega t})$

APPENDIX C

WKB ANALYSIS

We consider the following ordinary differential equation :

$$\frac{d^2u}{dz^2} - \lambda Q(z)u = 0 \quad (\lambda = \frac{a^2}{\sigma^2}) \quad 0 < z < 1 \tag{C.1}$$

$$u = 0 \quad z = 0, 1 \tag{C.2}$$

where $Q(z) = \frac{d\bar{\theta}(z)}{dz} + \sigma^2$

Note that $\frac{d\bar{\theta}(z)}{dz}$ is a monotonic decreasing function of z which changes sign in the interval $(0, 1)$ and that σ^2 is bounded by $-\frac{d\bar{\theta}(z)}{dz}$ at $z = 1$, otherwise the solution to the above system would be trivial. Since σ^2 must be positive we have a turning point for the above equation in the interval given. As $\lambda \to \infty$ we can apply WKB theory to get solutions to 2.6 away from the turning point.

On the interval $0 <= z < z_c$ where z_c is the turning point, u has the form:

$$u_I = \frac{A}{Q(z)^{\frac{1}{4}}} e^{(\lambda \int_z^{z_c} \sqrt{Q(\bar{z})} d\bar{z})} + \frac{B}{Q(z)^{\frac{1}{4}}} e^{(-\lambda \int_z^{z_c} \sqrt{Q(\bar{z})} d\bar{z})} \tag{C.3}$$

To satisfy condition that $u_I(0) = 0$ requires that u_I take the form:

$$u_I = \frac{A}{Q(z)^{\frac{1}{4}}} e^{(\lambda \int_z^{z_c} \sqrt{Q(\bar{z})} d\bar{z})} - e^{(-\lambda \int_z^{z_c} \sqrt{Q(\bar{z})} d\bar{z} + 2\lambda \int_0^{z_c} \sqrt{Q(\bar{z})} d\bar{z})} \tag{C.4}$$

but this solution blows up away from the boundary as $\lambda \to \infty$. Therefore, the solution u_I is equal to zero

Let u_{II} denote the solution just about the turning point. To study behavior of the solution about turning point let $z' = (Q'(z_c))^{\frac{1}{3}}(z - z_c)\lambda^{\frac{2}{3}}$. The governing differential equation for u in terms of z' becomes:

$$\frac{d^2u}{dz'^2} - z'u = 0 \tag{C.5}$$

$$u_{II} = BAi(z') \tag{C.6}$$

Note that $Ai(z') \to 0$ as $z' \to \infty$ which is consistent with our conjecture on u_I (see Bender and Orszag). As $z' \to -\infty$ u_{II} looks like:

$$u_{II} = \frac{Csin(\frac{2}{3}(-z')^{\frac{3}{2}} + \frac{\pi}{4})}{\sqrt{\pi}(-z')^{\frac{1}{4}}} \tag{C.7}$$

The solution u_{III} of region III ($z_c < z < 1$) has the form:

$$u_{III} = \frac{C}{-Q(z)^{\frac{1}{4}}} sin(\lambda \int_z^1 \sqrt{-Q(\tilde{z})}d\tilde{z}) + \frac{C}{-Q(z)^{\frac{1}{4}}} cos(\lambda \int_z^1 \sqrt{-Q(\tilde{z})}d\tilde{z}) \tag{C.8}$$

The boundary condition $u_{III}(1) = 0$ requires that u_{III} have the following form:

$$u_{III} = \frac{C}{-Q(z)^{\frac{1}{4}}} sin(\lambda \int_z^1 \sqrt{-Q(\tilde{z})}d\tilde{z}) \tag{C.9}$$

We must now match u_{III} as z moves toward the turning pt ($z = z_c$) with u_{II} as z moves toward $z = 1$. The solution u_{III} can be written as:

$$u_{III} = \frac{C}{-Q(z)^{\frac{1}{4}}} sin(\lambda(\int_{z_c}^1 \sqrt{-Q(\tilde{z})}d\tilde{z} - \int_{z_c}^z \sqrt{-Q(\tilde{z})}d\tilde{z})) \tag{C.10}$$

A matching of the Airy solution u_{II} with u_{III} requires that the constant expression, $\lambda \int_{z_c}^1 \sqrt{-Q(\tilde{z})}d\tilde{z} = 2n\pi + \frac{\pi}{4}$ for $\lambda >> 1$. ($n = \cdots -2, -1, 0, 1, 2 \cdots$). Hence, z_c must approach 1 for large disturbance wave numbers. For $z_c - z << 1$, $\lambda \int_{z_c}^z \sqrt{-Q(\tilde{z})}d\tilde{z}$ can be approximated and written in terms of z' as $2/3(-z')^{\frac{3}{2}}$. So near the turning point U_{II} exhibits the correct behavior to match with the Airy function. Recalling that $z_c \to 1$, the integral $\int_{z_c}^1 \sqrt{-Q(\tilde{z})}d\tilde{z}$ can be approximated by Taylor expanding $Q(z)$ about $z = 1$. The approximation in terms of θ and σ^2 is $\frac{2a^2(\frac{d\theta(1)}{dz}+\sigma^2)^{\frac{3}{2}}}{3\frac{d^2\theta}{dz^2}\sigma^2}$. Recalling that this expression equals a constant, we arrive at the following equation:

$$\frac{\frac{d\theta(1)}{dz} + \sigma^2}{\sigma^{\frac{4}{3}}} = \frac{3\pi/8\frac{d^2\theta(1)}{dz^2}^{2/3}}{a^{4/3}} \tag{C.11}$$

Note as $a \to \infty$ $\sigma^2 \to -\frac{d\theta(1)}{dz}$.

REFERENCES

1. Chandrasekhar S. 1981 *Hydrodynamic and Hydromagnetic Stability.* Dover Publications Inc., New York, NY.

2. Drazin P. G., Reid W. H. 1981 *Hydrodynamic Stability.* Cambridge University Press, New York, NY.

3. Fang C. S., Lai P. M. C. 1995 Microwave heating and separation of water-in-oil emulsions. *Journal of Microwave Power and Electromagnetic Energy.* **30**, 46–57.

4. Hippel A. V. 1954 *Dielectric Materials and Applications.* John Wiley and Sons Inc., New York, NY.

5. Kriegsmann G. A. 1992 Thermal runaway in microwave heated ceramics: A one-dimensional model. *Journal of Applied Physics.* **71**, 1960-1966.

6. Kriegsmann G. A. 1993 Microwave heating of dispersive media. *SIAM Journal of Applied Mathematics.* **53**, 655-669.

7. Kulacki F. A., Goldstein R. J. 1972 Thermal convection in a horizontal fluid layer with uniform volumetric Energy Sources. *Journal of Fluid Mechanics.* **55**, 271–257.

8. Pellow A., Southwell R. V. 1940 On convective motion in a fluid heated from below. *Proc. R. Soc.* **A176**, 312-343.

9. Ramo S., Whinnery J. R., Van Duzer T. 1984 *Fields and Waves in Communication Electronics.* John Wiley and Sons Inc., New York, NY.

10. Eds. Donnelly, R. J., Herman, R., Prigogine, I. 1966 *Non-equilibrium Thermodynamics, Variational Techniques and Stability.* University of Chicago Press, Chicago, IL.

11. Roberts, P. H. 1967 Convection in horizontal layers with internal heat generation theory. *Journal of Fluid Mechanics.* **30**, 33–49.

12. Sparrow, E. M., Goldstein, R. J. and Jonnson, V. K. 1964 Thermal instability in a horizontal layer: Effect of boundary conditions and non-linear temperature profile. *Journal of Fluid Mechanics.* **18**, 513–528.

13. Stuerga D., Lallemant M. 1993a An original way to select and control hydrodynamic instabilities: Microwave heating. Part I: Hydrodynamic background and the experimental set-up. *Journal of Microwave Power and Electromagnetic Energy.* **28**, 206–218.

14. Stuerga D., Lallemant M. 1993b An original way to select and control hydrodynamic instabilities: Microwave heating. Part II: Hydrodynamic behavior of water and ethanol under microwave heating and reduced pressure. *Journal of Microwave Power and Electromagnetic Energy.* **28**, 219-233.

15. Stuerga D., Lallemant M. 1994 An original way to select and control hydrodynamic instabilities: Microwave heating (Part IV). *Journal of Microwave Power and Electromagnetic Energy.* **29**, 3-30.

16. Stuerga D., Lallemant M., Steichen-Sanfeld A. 1994 An original way to select and control hydrodynamic instabilities: Microwave heating (Part III). *Journal of Microwave Power and Electromagnetic Energy.* **29**, 3-19.

17. Stuerga D., Lallemant M. 1994 An original way to select and control hydrodynamic instabilities: Microwave heating (Part IV). *Journal of Microwave Power and Electromagnetic Energy.* **29**, 20-30.

18. Tveitereid, M. and Palm, E. 1976 Convection due to internal heat sources. *Journal of Fluid Mechanics.* **76**, 481-499.

19. Watson P. M. 1968 Classical cellular convection with a spatial heat source. *Journal of Fluid Mechanics.* **32**, 399-411.

20. Yučel A., Bayazitoğlu, Y. 1979 Onset of convection in fluid layers with non-uniform volumetric energy sources. *Transactions of the ASME, Journal of Heat Transfer.* **101**, 666–671.

21. Hill James M., Dewynne Jeffrey N. 1987 *Heat Conduction.* Blackwell Scientific Publications., Boston, MA.

22. Crank J. 1984 *Free and Moving Boundary Problems.* Clarendon Press., Oxford, England.

23. Stuerga D., Zahreddine I., More C., Lallemant M. 1993 Bistable behavior in microwave heating: The first experimental evidence. *C. R. Acad. Sci. Paris*, t. **316**, **Series II**, 901–906.

24. Nachman M., Turgeon G. 1984 Heating pattern in a multi-layered material exposed to microwaves. *IEEE Transactions on Microwave Theory and Techniques*, **MTT-32 NO. 5**, 547–552.

25. Streit U. 1991 One-dimensional implicit moving boundary value problems: A new front tracking approach. *Numer. Funct. Anal. and Optimiz.*, **12(2 and 4)**, 413–428.

26. Sethian J. A., Strain J. 1992 Crystal growth and dendritic solidification. *Journal of Computational Physics.*, **98**, 231–253.

27. Smith G. D. 1993 *Numerical Solution of Partial Differential Equations: Finite Difference Methods.* Oxford University Press Inc., New York, NY.

28. Burden R. L., Faires J. D. 1989 *Numerical Analysis.* PWS-KENT Publishing Company, Boston, MA.

29. Rubinstein L. I. 1971 *The Stefan Problem.* American Mathematical Society, Providence, RI.

30. Goodman T. R. 1958 The heat-balance integral and its application to problems involving a change of phase. *Transactions of the ASME.*, **February**, 335–342.

31. Boley B. A. 1961 A method of heat conduction analysis of melting and solidification problems. *J. Math. Phys..*, **40**, 300–313.

32. Crank I. 1957 Two methods for the numerical solution of moving-boundary problems in diffusion and heat flow. *Quart. J. Mech. Appl. Math..*, **10**, 220–231.

33. Douglas J., Jr. 1957 A uniqueness theorem for the solution of a stefan problem. *Proc. Amer. Math. Soc..*, 8, 402–408.

34. Friedman A. 1959 Free boundary problems for parabolic equations. I, Melting of solids. *J. Math. Mech.*, 8, 499-517.

35. Feynman R.P., Leighton R.B., Sands M. 1964 *The Feynman Lectures on Physics.* Addison-Wesley Publishing Company, Reading, MA.